AGU PUBLICATIONS

Journal of Advances in Modeling Earth Systems

RESEARCH ARTICLE

10.1002/2014MS000344

Modeling methane emissions from arctic lakes: Model development and site-level study

Zeli Tan[1], Qianlai Zhuang[1,2], and Katey Walter Anthony[3]

[1]Department of Earth, Atmospheric, and Planetary Sciences, Purdue University, West Lafayette, Indiana, USA, [2]Department of Agronomy, Purdue University, West Lafayette, Indiana, USA, [3]Water and Environmental Research Center, University of Alaska Fairbanks, Fairbanks, Alaska, USA

Key Points:
- CH4 emissions from lakes can be modeled by using a process-based model
- Bubbling rate controlling N2 strippig predominantly determines CH4 concentration
- The thawing of organic-rich yedoma permafrost can fuel sediment methanogenesis

Supporting Information:
- Supporting Information S1

Correspondence to:
Q. Zhuang,
qzhuang@purdue.edu

Citation:
Tan, Z., Q. Zhuang, and K. W. Anthony (2015), Modeling methane emissions from arctic lakes: Model development and site-level study, *J. Adv. Model. Earth Syst.*, *07*, doi:10.1002/2014MS000344.

Received 12 MAY 2014
Accepted 21 MAR 2015
Accepted article online 27 MAR 2015

Abstract To date, methane emissions from lakes in the pan-arctic region are poorly quantified. In order to investigate the response of methane emissions from this region to global warming, a process-based climate-sensitive lake biogeochemical model was developed. The processes of methane production, oxidation, and transport were modeled within a one-dimensional sediment and water column. The sizes of ^{14}C-enriched and ^{14}C-depleted carbon pools were explicitly parameterized. The model was validated using observational data from five lakes located in Siberia and Alaska, representing a large variety of environmental conditions in the arctic. The model simulations agreed well with the measured water temperature and dissolved CH_4 concentration (mean error less than 1°C and 0.2 μM, respectively). The modeled CH_4 fluxes were consistent with observations in these lakes. We found that bubbling-rate-controlling nitrogen (N_2) stripping was the most important factor in determining CH_4 fraction in bubbles. Lake depth and ice cover thickness in shallow waters were also controlling factors. This study demonstrated that the thawing of Pleistocene-aged organic-rich yedoma can fuel sediment methanogenesis by supplying a large quantity of labile organic carbon. Observations and modeling results both confirmed that methane emission rate at thermokarst margins of yedoma lakes was much larger (up to 538 mg CH_4 m^{-2} d^{-1}) than that at nonthermokarst zones in the same lakes and a nonyedoma, nonthermokarst lake (less than 42 mg CH_4 m^{-2} d^{-1}). The seasonal variability of methane emissions can be explained primarily by energy input and organic carbon availability.

1. Introduction

Methane (CH_4) is the second most powerful carbon-based greenhouse gas in the atmosphere behind carbon dioxide (CO_2). It also plays a significant role in the production of ozone (O_3) and reduction of hydroxyl radicals (OH) [*Forster et al.*, 2007; *Denman et al.*, 2007]. With the outburst of emissions from human activities, perhaps exacerbated by natural emissions, the global CH_4 burden has more than doubled since preindustrial times [*Etheridge et al.*, 1998]. Earlier studies have demonstrated that large releases of CH_4 from natural sources during warming events exert significant positive effects on atmospheric CH_4 levels and may have potential synergistic effects leading to aggravated or sustained global warming [*Dlugokencky et al.*, 2001, 2009; *Fisher et al.*, 2011; *Kort et al.*, 2012; *Zhuang et al.*, 2004]. Observations and climate model projections both confirm that arctic land north of 65°N is one of the most prominent global warming region, with a warming more than a factor of two greater than the global mean value in the past decades [*Hansen et al.*, 2007] and of a 2–7.5°C temperature increase by 2100 [*Intergovernmental Panel on Climate Change*, 2013]. Large reservoirs of organic carbon (C), currently sequestered in permafrost soils (~1466 Pg) [*Tarnocai et al.*, 2009], could be mobilized in the production and release of CO_2 and CH_4 from wetlands, lakes, and rivers, with magnitude more intensive than previously predicted [*Isaksen et al.*, 2011; *Schuur et al.*, 2011; *Harden et al.*, 2012; *MacDougall et al.*, 2012]. Furthermore, since lakes are a prominent landscape feature in the arctic, occupying up to 30% of land surface area [*Zimov et al.*, 1997; *Semiletov*, 1999; *Riordan et al.*, 2006], and could increase by 15–25% in coverage by 2100 due to thawing permafrost [*van Huissteden et al.*, 2011; *Gao et al.*, 2013], CH_4 emissions from arctic lakes could represent a potentially large and increasing source of greenhouse gases. Until now, CH_4 emissions from pan-arctic lakes are poorly quantified. Earlier studies that aimed to assess CH_4 emissions from lakes showed that heterogeneity in ebullition is a major obstacle to estimation accuracy [*Casper et al.*, 2000; *Bastviken et al.*, 2004; *Walter Anthony and Anthony*, 2013]. This contributes to the large uncertainty in the global lake CH_4

emission estimates: 1–25 Tg CH_4 yr^{-1} by *Cicerone and Oremland* [1988], 36–51 Tg CH_4 yr^{-1} by *Casper et al.* [2000], 8–48 Tg CH_4 yr^{-1} by *Bastviken et al.* [2004], and 103 Tg CH_4 yr^{-1} by *Bastviken et al.* [2011]. Furthermore, this lake CH_4 source has often been ignored from regional estimates of natural CH_4 emissions. For instance, *Walter et al.* [2006] indicated that when incorporating CH_4 emissions from northern Siberian thermokarst (thaw) lakes, the total CH_4 efflux from this region can increase significantly by 10–63%. Including CH_4 emissions from lakes increased the previous estimate of natural CH_4 sources in Alaska by 50–70% [*Walter Anthony et al.*, 2012]. *Walter et al.* [2007] projected that CH_4 emissions from northern high-latitude lakes, which were estimated to be 14–35 Tg CH_4 yr^{-1}, could rise to a level as high as 50 to 100 Tg CH_4 yr^{-1}, given that yedoma permafrost thaws over a timescale of centuries to millennia.

To date, regional estimates of CH_4 fluxes from lakes have been based on a limited number of site measurements using simple extrapolation techniques (e.g., bookkeeping approach) [*Bastviken et al.*, 2004; *Walter et al.*, 2006, 2007; *Zimov et al.*, 1997; *Gao et al.*, 2013]. Since the processes resulting in CH_4 production and release into the atmosphere depend highly and nonlinearly on the climate, those simple methods will result in a large uncertainty in future CH_4 emission estimates. Recently, several numerical lake models have been developed to estimate CH_4 effluxes from lakes in the permafrost zone by incorporating vital processes of permafrost thaw and CH_4 cycling [*Kessler et al.*, 2012; *Stepanenko et al.*, 2011]. For example, *Greene et al.* [2014] demonstrated the importance of winter ice cover impeding ebullition fluxes to the atmosphere, causing 80% of bubble CH_4 content to diffuse into the lake water column before bubbles are encapsulated in lake ice. However, one or more important processes that determine CH_4 content in ebullition bubbles have still been missed in these existing models, such as N_2 stripping [*Walter et al.*, 2008], sediment depth of bubble origin [*Walter et al.*, 2008], water column gas exchange with bubbles [*Leifer and Patro*, 2002; *McGinnis et al.*, 2006], and the role of ice cover in reducing water column thickness in winter. The objective of this study is to develop a process-based, climate-sensitive lake biogeochemical model that explicitly incorporates lake thermal dynamics, permafrost freeze-thaw dynamics, CH_4 production and consumption, and gas transport within sediment and water columns [*MacKay et al.*, 2009]. This model will be capable of quantifying the impact of climate on CH_4 emissions from pan-arctic lakes and the impact of N_2 stripping and water-bubble gas exchange on CH_4 content in bubbles during both ice-free and ice-cover seasons. Model sensitivity to parameters was tested with a variance-based method [*Sobol'*, 1993], and poorly constrained parameters were calibrated with the SCE-UA global optimization algorithm [*Duan et al.*, 1994]. Model validity was verified by comparing simulated and observed lake temperature, dissolved CH_4 concentrations, and CH_4 emissions of several thermokarst and nonthermokarst lakes in Alaska and Siberia.

2. Methods

2.1. Model Description

2.1.1. Overview

Since the processes controlling CH_4 emissions from pan-arctic lakes occur in both water and sediments, the lake biogeochemical model (bLake4Me) is structured as follows (Figure 1): one-dimensional (1-D) sediment and water columns are divided into 10 cm thick parallel layers. CH_4 is produced by anaerobic reactions in sediments (including methanogenesis) and consumed by aerobic reactions in oxygenated portions of the water column (methanotrophy). For simplicity, the oxidation of CH_4 by alternative electron acceptors, such as SO_4, is not included. The methanogenic and methanotrophic rates at each layer are modeled as functions of layer temperature and substrate concentrations. Within each layer of the two columns, temperature and dissolved gas concentrations (CH_4 and N_2 in sediments; N_2, O_2, CO_2, and CH_4 in water) are calculated by solving 1-D thermal and gas diffusion equations. The water phase change in the two columns is driven by the heat gain/loss of lake water to air above and to lake sediment underlain by permafrost below. In winter, ice grows downward from the top of the water column when layer temperature falls below 0°C; along shallow shores, the seasonal ice layers can extend into sediments. The formation of ice allows snow to accumulate in winter. The growth and decline rates of a single snow layer depend on snow fall, compaction, sublimation, and melting [*Fang and Stefan*, 1994]. In summer, heat penetrates sediments to thaw permafrost beneath the lake, facilitating the growth of a thaw bulb (talik) [*Ling and Zhang*, 2003; *West and Plug*, 2008].

With CH_4 is produced by methanogens, its concentration in a sediment layer grows until it exceeds the saturation threshold. Once above the saturation threshold, the excess CH_4 enters bubbles and escapes sediments into the water column via bubbling. Yedoma thermokarst lakes were formed in the thick

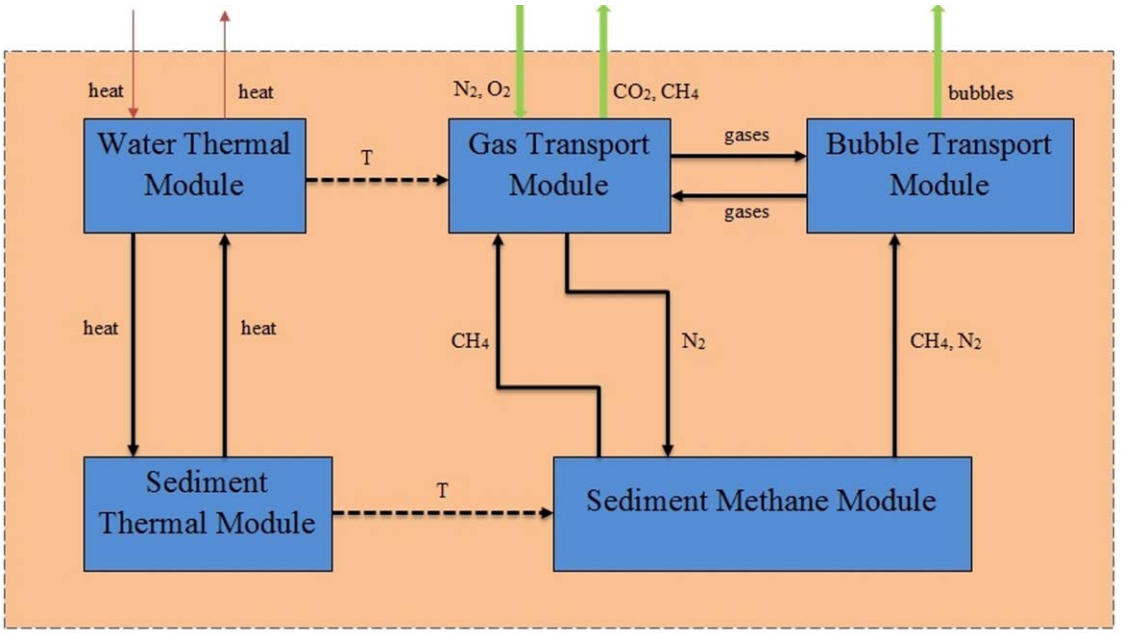

Figure 1. The framework of the bLake4Me model (The lake model includes a water thermal model (WTM), a sediment thermal model (STM), a gas transport model (GTM), a sediment gas model (SGM), and a bubble transport model (BTM); the solid arrow indicates energy or substance transport and the dashed arrow indicates process dependence).

Pleistocene-aged, organic-rich, silty ice complex known as "yedoma" [*Zimov et al*., 1997]. Their surface sediments heat up in summer and release more bubbles with younger ^{14}C-age CH_4 via partial acetate fermentation [*Walter et al*., 2006, 2008]. Conversely, due to the lag effects of heat diffusion, deeper talik sediments warm up in later winter/early spring, releasing CH_4 bubbles consistently via CO_2 reduction with older ^{14}C ages [*Walter et al*., 2006, 2008]. With permafrost thawing at depth, an additional labile carbon substrate is added to deep sediments for methanogens [*Walter Anthony et al*., 2010; *Sepulveda-Jauregui et al*., 2014]. As described by previous field studies [*Scandella et al*., 2011a] and lab experiments [*Scandella et al*., 2011b], when a sufficient volume of CH_4 is produced or when the hydrostatic pressure drops enough to dislocate large bubbles in fine-grain sediments, the bubbles can break out, creating preferential flow channels (bubble tubes). Through those tubes, bubbles formed in deep sediments can escape the sediment column without losing much CH_4 to pore water by dissolution. For nonyedoma lakes, bubbles are likely produced predominantly in surface sediments from newly deposited organic matter (OM) [*Wik et al*., 2014]. For nonthermokarst lakes, the transport of OM to surface sediments from bank erosion could be relatively more limited [*Wik et al*., 2014] especially when wind-driven bank erosion is inactive. Field studies reported that CH_4 and N_2 in bubbles were negatively correlated in Siberian and Alaskan lakes [*Walter et al*., 2008]. Following similar observations in peatlands [*Chanton et al*., 1989], *Walter et al*. [2008] attributed this negative correlation in lakes to N_2 stripping. When the rate of bubbling from sediments exceeds the rate of N_2 diffusion into sediments, gas exchange between sediment pore water and free-phase bubbles depletes dissolved pore-water N_2, resulting in N_2-poor/CH_4-rich bubbles released from sediments. Thus bubbles collected at the lake surface from high-flux ebullition seeps with deep sediment origins had high CH_4/N_2 ratios. In contrast, when CH_4 is produced in shallow sediments of Siberian and Alaskan lakes (low-flux point-source seeps and background bubbling), where bubbling is slower and dissolved N_2 concentrations are relatively higher, released bubbles had lower CH_4/N_2 ratios [*Walter et al*., 2008].

In our process-based model, the concentrations of bubble gases are modeled with continuity equations. This approach is similar to that of *Liang et al*. [2011] for modeling bubbles and dissolved gases in the ocean. In a single bubble, gas concentrations are determined by hydrostatic pressure, bubble diameter in the water column, and ambient dissolved gas concentrations.

2.1.2. Water and Sediments Thermal Dynamics Model

The thermal dynamics of a lake body is governed by heat exchange between lake water and the air above. At the surface, the water body gains or loses energy by thermal radiation, latent heat flux, and sensible heat

flux. Within the water column, except subsurface heating by the absorption of incident solar radiation, the heat flow is dominated by wind-driven eddy diffusion, molecular diffusion, and buoyant convection [*MacIntyre et al*., 2009]. The sediment column typically gains or loses heat solely from or to the water above it, and its internal heat transport is driven only by molecular diffusion. Water phase change in the two columns is also explicitly parameterized.

The governing 1-D thermal diffusion equation for the water column is [*Hostetler and Bartlein*, 1990]:

$$\frac{\partial T_w}{\partial t}=\frac{1}{A}\frac{\partial}{\partial z}\left(A(D_m+D_e)\frac{\partial T_w}{\partial z}\right)+\frac{1}{A}\frac{1}{\rho_w c_{pw}}\frac{\partial[\Phi A]}{\partial z} \tag{1}$$

where T_w is the water temperature (K), t the is time (s), z is the depth from the lake surface (m), A is the area of lake cross section (m^2), D_m is the molecular diffusivity of water ($m^2\ s^{-1}$), D_e is the wind-driven eddy diffusivity ($m^2\ s^{-1}$), Φ is the incoming solar radiation (W m^{-2}), ρ_w is the water density (kg m^{-3}), and c_{pw} is the specific heat of water (J $kg^{-1}\ K^{-1}$). As described by *Hostetler and Bartlein* [1990], the area of water cross section A is a function of water depth and also depends on the lake shape. In the model, we confine the area effect just in the marginal areas of a lake and assume that the dimension of water cross section decreases linearly with depth. The heat diffusion of a lake water body can be highly amplified by surface wind movement during ice-free seasons [*MacIntyre et al*., 2009]. In our model, we follow the method of many existing lake models by defining this amplification as a wind-driven eddy diffusivity D_e, which is evaluated at each layer as a function of 2 m wind speed, the Brunt-Väisälä frequency implied by lake density profile ($N=[-g/\rho_w(\partial\rho/\partial z)]^{1/2}$), and a latitude-dependent Ekman decay parameter [*Hostetler and Bartlein*, 1990]. The solar radiation term in equation (1) is calculated in accordance with Beer's law as

$$\Phi=(1-\beta)L_0 e^{-\eta z} \tag{2}$$

where β is the proportion of shortwave radiation that is reflected by water, L_0 is the incident solar radiation at lake surface (W m^{-2}), and η is the light extinction coefficient of lake water (m^{-1}). In the work of *Subin et al*. [2012], η was defined as a simple empirical function of lake depth using the Poole-Atkins expression:

$$\eta=1.1925d^{-0.424} \tag{3}$$

where d is the lake depth (m). Equation (3) reflects a negative correlation between lake trophic status and depth. However, as implied by the measurements at Lake Kossenblatter, Valkea-Kotinen, and Karujärv [*Subin et al*., 2012], this formula can severely underestimate the light extinction coefficient of high-latitude shallow lakes, causing lake models to overstate heat pulse effect in sediments. In this model, we modified the original equation by introducing a trophic state factor λ for shallow lakes ($\lambda \geq 1$).

The top boundary condition couples equation (1) with the balance of in-and-out heat fluxes at the lake surface [*Hostetler and Bartlein*, 1990]:

$$k_w\frac{\partial T}{\partial z}=(1-\beta)L_0+L_d-L_u\pm Q_e\pm Q_h \tag{4}$$

where k_w is the heat conductivity of water ($=\rho_w c_{pw}(D_m+D_e)$), L_d is the incident thermal radiation (W m^{-2}), L_u is the emergent thermal radiation (W m^{-2}), Q_e is the latent heat flux from lake (W m^{-2}), and Q_h is the sensible heat flux from lake (W m^{-2}). The heat terms in equation (4) are parameterized with the formulae given by *Hostetler and Bartlein* [1990]. For lakes in the pan-arctic region, heat exchange between the lake sediment and water columns normally exists. Thus, the bottom boundary condition of equation (1) is given by assuming heat balance at the water-sediment interface:

$$k_w\frac{\partial T_w}{\partial z}\Big|_{bottom}=k_s\frac{\partial T_s}{\partial z}\Big|_{top} \tag{5}$$

where T_s is the sediment temperature (K) and k_s is the heat conductivity of sediment on the boundary (W $m^{-1}\ K^{-1}$). For small arctic lakes, the lateral heat flow driven by wind is assumed to be negligible [*Fang and Stefan*, 1994; *Stepanenko et al*., 2011]. The heat flow driven by a horizontal temperature gradient between the lake and surrounding permafrost at marginal areas is addressed by applying water freezing temperature at the periphery of the lake, a method similar to that of *West and Plug* [2008].

During spring and fall, water temperature instabilities (i.e., warmer water underlying colder water) could trigger convective mixing of the whole water column. We employ a scheme after *Hostetler and Bartlein* [1990] to emulate this process, in which the distribution of extra energy to adjacent layers was assumed to occur immediately and recursively until the between-layer temperature difference is less than a small specified-value.

Snow thickness is determined by taking account of snow accumulation due to snow fall, snow compaction due to gravity, and snow melting due to heat conduction, longwave radiation, shortwave radiation, and rainfall [*Fang and Stefan*, 1994].

The governing diffusion equation for heat transfer in sediments is [*Fang and Stefan*, 1998]:

$$c_{vs}\frac{\partial T_s}{\partial t}=\frac{\partial}{\partial z}\left(k_s\frac{\partial T_s}{\partial z}\right) \tag{6}$$

where c_{vs} is the volumetric heat capacity of sediments (J m^{-3} K^{-1}), defined as a sum of heat capacity of sediment components ($c_{vs}=\rho_w c_{pw}\theta+\rho_i c_{pi}\theta_i+\rho_s c_{ps}(1-\theta-\theta_i)$, where ρ_i and ρ_s are the densities of ice and sediment solid particles (kg m^{-3}), c_{pi} and c_{ps} are the specific heat of ice and sediment solid particles (J kg^{-1} K^{-1}), θ is the water content, and θ_i is the ice content). As the heat conductivity of soils was observed to amplify dramatically when the water content starts to freeze [*Hansson et al*., 2004], the parameterization of k_s in the bLake4Me model was handled with different equations based on the water and ice contents. For the ice-free or totally frozen sediments, k_s is calculated using equations provided by *Farouki* [1981]. For the partially thawed sediments at the thaw-bulb front, k_s is formulated as a nonlinear function of sediment water and ice contents proposed by *Hansson et al*. [2004]:

$$k_s=\begin{cases} k_w a^2+k_{solid}(1-a)^2+\{k_w k_{solid}(2a-2a^2)/[k_{solid}a+k_w(1-a)]\} & T_s>0 \\ C_1+C_2(\theta+F\theta_i)-(C_1-C_4)\exp\left\{-[C_3(\theta+F\theta_i)]^{C_5}\right\} & T_s=0 \\ k_i a^2+k_{solid}(1-a)^2+\{k_i k_{solid}(2a-2a^2)/[k_{solid}a+k_i(1-a)]\} & T_s<0 \end{cases} \tag{7}$$

where k_i is the heat conductivity of ice, k_{solid} is the heat conductivity of sediment solid particle, a is a function of porosity, and $F=1+F_1\theta_i^{F_2}$ ($C_1=0.55$, $C_2=0.8$, $C_3=3.07$, $C_4=0.13$, $C_5=4.0$, $F_1=13.05$, and $F_2=1.06$). High-flux gas bubbles could offset k_s from equation (7) in two ways: (1) bubble movement in sediments could accelerate heat transfer, increasing k_s; and (2) the much lower heat conductivity of bubble gases compared to water could decrease k_s. Using the equation of *De Vries* [1963], when assuming 5–15% gas-filled porosity [*Strack et al*., 2005], the second effect alone can lower k_s by 5.4–16.6%. The change of k_s due to bubble movement is hard to estimate, but it could be larger than the second one in high CH_4 flux zones of lakes. Thus, it is necessary to incorporate the effect of gaseous bubbles into equation (7) to better simulate heat transfer in yedoma-lake sediments in future model development.

The variability of sediment temperatures is primarily driven by the heat exchange occurring at the water-sediment interface, as presented in equation (5). At the bottom of sediments, heat flux is negligible:

$$k_s\frac{\partial T_s}{\partial z}=0 \tag{8}$$

The initial temperature of sediment bottom is derived from the annual mean air temperature [*Fang and Stefan*, 1998]. The mean annual temperature of lake bottom (surface sediments) could be determined by climate, lake size, and lake ice but precise relationships are not yet available. We assign initial temperatures to the bottoms of Lake Shuchi, Tube Dispenser, Goldstream, Claudi, and Toolik (Table 1) from field measurements (K. M. Walter Anthony, unpublished data, 2013) [*Giblin et al*., 2010].

2.1.3. Sediment Biogeochemical Model

As sediment environment is highly anoxic and CO_2 has high solubility, both O_2 and CO_2 were found to contribute trivial amounts of bubble volume by field measurements [*Walter et al*., 2008]. Thus, gas concentrations in sediments are calculated by solving only two 1-D gas diffusion equations involving CH_4 production and the diffusion and ebullition of CH_4 and N_2:

Table 1. Lake Characteristics and Observation Data Types at Study Sites

Site Name	Location	Max Depth (m)	Area (ha)	Classification[a]	Observations[b]	Sources[c]
Goldstream Lake	64.9°N/147.7°W	2.9	1.0	C1	WT, ST	UAF
Shuchi Lake	69°N/161°E	11.0	5.8	C2	AP, E	NCEAS, UAF
Tube Dispenser Lake	69°N/161°E	17.0	11.0	C2	AP, E	NCEAS, UAF
Claudi Lake	66.6°N/164.5°W	10.0	16.3	C3	E	UAF
Toolik Lake	68.4°N/149.4°W	25.0	149.0	C4	E	UAF

[a]C1, boreal, discontinuous permafrost, yedoma-type; C2, tundra/taiga treeline, continuous permafrost, yedoma; C3, tundra, continuous permafrost, yedoma; and C4, kettle lake formed in continuous permafrost, nonyedoma lake. C1 to C3 are thermokarst lakes.
[b]WT, water temperature; ST, sediment temperature; AP, air pressure; and E, ebullition.
[c]UAF, Water and Environmental Research Center at University of Alaska, Fairbanks [*Walter Anthony and Anthony*, 2013]; NCEAS, NCEAS Project 10646 [*Walter et al*., 2008; http://www.nceas.ucsb.edu/projects/10645].

$$\frac{\partial C_{CH_4,s}}{\partial t} = \frac{\partial}{\partial z}\left(D_{CH_4,s}\frac{\partial C_{CH_4,s}}{\partial z}\right) + P - \alpha_{CH_4}E \tag{9}$$

$$\frac{\partial C_{N_2,s}}{\partial t} = \frac{\partial}{\partial z}\left(D_{N_2,s}\frac{\partial C_{N_2,s}}{\partial z}\right) - \alpha_{N_2}E \tag{10}$$

where $C_{CH_4,s}$ and $C_{N_2,s}$ are the CH_4 and N_2 concentrations in sediments (μmol m^{-3}); $D_{CH_4,s}$ and $D_{N_2,s}$ are the CH_4 and N_2 diffusivity in porous medium (m^2 s^{-1}); P is the CH_4 production rate from anaerobic decomposition of organic carbon (μmol m^{-3} s^{-1}); E is the gas loss rate due to ebullition (μmol m^{-3} s^{-1}); α_{CH_4} and α_{N_2} are CH_4 and N_2 percentage in bubbles. Rather than incorporating CH_4 alone as done by *Stepanenko et al*. [2011], the addition of N_2 in the sediment biogeochemical module should be in favor of understanding CH_4 percentage variability in bubbles [*Walter et al*., 2008; *Walter Anthony et al*., 2010]. As suggested by *Walter and Heimann* [2000], column-average gas diffusivity in sediments is defined as a function of sediment coarse pore fraction (0.3–0.6) [*Hillel*, 1980; *Cornwell and Kipphut*, 1992; *Audry et al*., 2011]. We also assume that CH_4 and N_2 cannot enter or escape the sediment column from its bottom; rather, sediment N_2 is fed by gas diffusion from the atmosphere via the water column, and N_2 is not produced or consumed in sediments.

CH_4 production by methanogenic Archaea (methanogenesis) has two major pathways: CO_2 reduction and acetate fermentation [*Nakagawa et al*., 2002; *Barber*, 2007]. As acetate fermentation requires a higher activation energy than CO_2 reduction [*Barber*, 2007], the former is favored in the environment with high availability of labile organic substrates and high temperature, e.g., top sediment layers in summer. In contrast, CO_2 reduction has been observed in deep sediment layers where temperature is low and organic matter quality may vary, as well in upper sediment layers [*Walter et al*., 2008]. Accordingly, we partition the CH_4 production on the basis of two carbon pools in the pan-arctic region: new organic matter is added at the water-sediment interface (young ^{14}C-enriched organic carbon pool) and old organic matter added from thawing permafrost (old ^{14}C-depleted organic carbon pool). For yedoma lakes, both carbon pools contribute to CH_4 production in the surface sediments and the permafrost thaw bulb under lakes. For nonyedoma lakes, only the ^{14}C-enriched carbon pool is responsible for CH_4 production in surface lake sediments. Without considering carbon quality, the methanogenic activities of two pathways depend on the same factors: organic carbon availability, soil temperature, soil pH, and redox potentials [*Walter and Heimann*, 2000; *Zhuang et al*., 2004]. Since lake sediments are totally inundated and their pH and redox potentials are unknown, we simplify CH_4 production rate as a function of labile carbon content and temperature [*Kessler et al*., 2012]:

$$P = R_C \cdot C_{labile} \cdot PQ_{10}^{\left(T-T_{pr}\right)/10} \tag{11}$$

where R_c is the fraction of carbon converted per year, C_{labile} is the labile carbon density (μmol m^{-3}), PQ_{10} is a factor by which the production rate increases with a 10°C rise in temperature, and T_{pr} is a reference temperature of CH_4 production. The model distinguishes two carbon pools with different pool parameters: $R_{c,new}$, $PQ_{10,new}$, and $T_{pr,new}$ for the ^{14}C-enriched carbon pool within near-surface sediments, and $R_{c,old}$, $PQ_{10,old}$, and $T_{pr,old}$ for the ^{14}C-depleted carbon pool within thawed deep permafrost sediments. The values of R_c and PQ_{10} are calibrated. $T_{pr,new}$ and $T_{pr,old}$ are set to 3.5 and 0°C respectively. We further assume that

CH_4 production completely shuts down when sediments freeze [*Walter and Heimann*, 2000]. The sizes of the two carbon pools are derived from the published incubation data of mineral soils in yedoma permafrost and arctic drained basins, and by linking with lake characteristics. According to *Walter et al.* [2007] and *Walter Anthony et al.* [2014], one-third of total carbon stock (C_{total}) in yedoma ice complex can be converted into labile carbon, half of which will be further decomposed to CH_4. In contrast, soil incubations show that 22% of shallow mineral soil carbon can be decomposed in aerobic conditions within 50 years [*Schädel et al.*, 2014], of which 23.1–33.3% will be reduced to CH_4 [*Hodgkins et al.*, 2014]. The pool size of ^{14}C-enriched carbon is determined by the deposition of both autochthonous carbon within the lake [*Rudd et al.*, 1978] and allochthonous carbon from terrestrial ecosystems [*Canham et al.*, 2004]. The supply of organic matter to surface lake sediments was reported as a function of lake shape [*Ferland et al.*, 2012], catchment soil organic matter [*Cole et al.*, 2007], site position (littoral versus profundal) [*Benoy et al.*, 2007], and permafrost condition (thermokarst margin versus nonthermokarst margin) [*Walter et al.*, 2006; *Kessler et al.*, 2012]. In the model, the ^{14}C-enriched carbon pool is derived by comparing the relative properties of each lake to the average values of 13 boreal lakes in northern Québec [*Ferland et al.*, 2012]. Following *Ferland et al.* [2012] and *Zhuang et al.* [2004], we define the effect of each factor on the pool size as a multiplier:

$$C_{tot,\ 14C-enriched} = \alpha_{erode}\ C_{tot,\ ref}\ f_{shape}(LA,\ LH)\ f_{pos}(h)\ \frac{SOM}{SOM_{ref}} \tag{12}$$

where $C_{tot,\ ref}$ is the average carbon stock (8.94 kg C m^{-2}) of the 13 Canadian boreal lakes, $f_{shape}(LA,\ LH)$ is a multiplier ($=(\sqrt{LA}/LH)^{-0.555}$) that defines the relationship of carbon stock to lake shape (*LA* is lake area (km^2) and *LH* is mean lake depth (m)) [*Ferland et al.*, 2012], $f_{pos}(h)$ is a multiplier that defines the negative correlation of carbon stock to oxygen exposure time (*h* is lake depth) [*Ferland et al.*, 2014], *SOM* is the average catchment soil carbon density of the studied lake, SOM_{ref} is the average catchment soil carbon density of the 13 Canadian lakes, and α_{erode} is a multiplier that represents the increase of carbon stock by thermokarst eroding. Studies also showed that the flooding of rivers or streams could dramatically alter the ^{14}C-enriched carbon pool [*Kelly et al.*, 1997] but it is not practical to model it by a lake model alone. Because the ^{14}C-enriched carbon is deposited continuously at the water-sediment interface, its pool size was deemed to decrease exponentially with a rate α_H (units: m^{-1}) from water-sediment interface to sediment bottom [*Walter and Heimann*, 2000; *Zhuang et al.*, 2004]. For the ^{14}C-depeleted carbon pool, its pool size is determined by the amount of total carbon stock in thawed lake talik and the decomposition rate of organic matter. *West and Plug* [2008] suggested that the thickness (m) of talik under lake can be rather accurately approximated by using a classical formula $C_t\sqrt{t}$, where *t* is a time from the initiation of a thermokarst lake (year) and C_t is a function of lake bottom temperature and sediment thermal conductivity [*Burn*, 2002]. The initial density of Pleistocene-aged organic matter in talik is assigned uniformly as 29.3 kg m^{-3} [*Schirrmeister et al.*, 2011].

In the model, regardless of pathways, the yield of bubbles is modeled with the same scheme. Assuming bubbles in sediments consist only of CH_4 and N_2, the sum of partial pressures of both gases should equal the hydrostatic pressure exerted on bubbles. Through this equivalence, *Stepanenko et al.* [2011] derived an equation that links the critical concentration of CH_4 ebullition to soil porosity, gas solubility, and hydrostatic pressure as:

$$C_{CH_4,cr}(p_a, h, C_{N_2}, \Pi) = \Pi K_{H,CH_4}(T) \times \left[p_a + \rho_w g h - C_{N_2}/K_{H,N_2}(T)\right] \tag{13}$$

where Π is the porosity of sediment, $K_{H,CH_4}(T)$ and $K_{H,N_2}(T)$ are the temperature-dependent henry constants of CH_4 and N_2 [*Segers*, 1998], P_a is air pressure, $\rho_w g h$ is the hydrostatic pressure of the water column, and C_{N_2} is the concentration of N_2 in pores. With the existence of capillary and osmotic forces, saturated CH_4 concentrations cannot be converted into bubbles instantly. The velocity of bubble formation depends on many factors, including pore size, ambient CH_4 concentration, and CH_4 diffusivity in pore water [*Algar and Boudreau*, 2009]. Bubbles measured at the surface of the studied lakes had diameters within 5–20 mm. By applying the bubble formation equation of *Algar and Boudreau* [2009] with typical factor values and the above diameter range, we estimate that the bubbles can be yielded at a rate varying from 1.1×10^5 to 1.5×10^6 s^{-1}. Although theoretically ebullition should start only when CH_4 concentration exceeds the threshold $C_{CH_4,cr}$, field studies in the past showed that it could be initiated well below saturation levels [*Baird et al.*, 2004]. By taking these findings into account, *Stepanenko et al.* [2011] proposed a formula of ebullition rate

that assumes CH_4 bubble formation is activated when dissolved CH_4 concentrations reach 40% of the saturation level:

$$E=\max\left\{0, c_e\left[C_{CH_4}-\alpha_e C_{CH_4,cr}(p_a, h, C_{N_2}, \Pi)\right]\right\} \tag{14}$$

where c_e is the velocity of bubble formation (s^{-1}) and $\alpha_e=0.4$ is the relative saturation level. For simplicity, CH_4 bubbles formed in sediments are assumed to have diameters in the range of 5–20 mm with a uniform distribution of surface tension when reaching the water-sediment interface.

2.1.4. Modeling Bubble Transport

In the model, four types of substances (N_2, O_2, CO_2, and CH_4) are assumed to be involved in the gas transport via diffusion and ebullition within water column [*Tang et al.*, 2010]. Earlier studies for simulating bubbles in oceans have tried to predict their evolution by modeling three processes: buoyant rising, gas exchange with ambient water, and bubble expansion [*Woolf and Thorpe*, 1991; *Liang et al.*, 2011]. The concentration of one gas in bubbles with radius r and location z is determined by a two-dimensional continuity equation [*Liang et al.*, 2011]:

$$\frac{\partial n_m(r,z,t)}{\partial t}=-\frac{\partial w^b n_m(r,z,t)}{\partial z}-\frac{\partial}{\partial r}\left(\frac{dr}{dt}n_m(r,z,t)\right)+\frac{dn_m}{dt}C_b(r,z,t) \tag{15}$$

where $n_m(r,z,t)$ is the concentration of gas m (m = 1, N_2; m = 2, O_2; m = 3, CO_2; m = 4, CH_4), w^b is the rising velocity of bubble at radius r, $C_b(r,z,t)$ is the number of bubbles at radius r and location z (equation (16)), $\frac{dr}{dt}$ is the bubble radius change rate (equation (17)), and $\frac{dn_m}{dt}$ is the gas exchange rate of a single bubble (equation (19)). According to *Woolf and Thorpe* [1991], w^b is a function of bubble radius and kinematic viscosity:

$$C_b(r,z,t)=\frac{3RT_w}{4P\pi r^3}\sum_m n_m(r,z,t) \tag{16}$$

where P is the total pressure exerted on bubble surface (equation (18)):

$$\frac{dr}{dt}=\left[\frac{3RT_w}{4\pi r^2}\sum_m\frac{dn_m}{dt}-r\frac{dp_l}{dt}\right]\left(3\rho_w gz+3p_a+\frac{4\gamma}{r}\right)^{-1} \tag{17}$$

where γ is the surface tension coefficient and $\frac{dp_l}{dt}=-\rho_w g w^b$ is the hydrostatic pressure decrease rate with bubble rising. The total pressure P is a sum of air pressure, hydrostatic pressure, and pressure added by a curved surface [*Liang et al.*, 2011]:

$$P=\rho_w gz+p_a+\frac{2\gamma}{r} \tag{18}$$

Gas exchange between bubbles and ambient water is driven by the gradient of gas partial pressure in and out of bubbles [*Thorpe*, 1982]:

$$\frac{dn_m}{dt}=-4\pi r D_m Nu_m\left[S_m X_m^b P-c_m\right] \tag{19}$$

where D_m, Nu_m, and S_m are the diffusivity, Nusselt number, and solubility of gas m, X_m^b is the mixing ratio of gas m in bubbles, and c_m is the concentration of gas m dissolved in ambient water. D_m, Nu_m, and S_m are all calculated following *Woolf and Thorpe* [1991].

Due to the kinetic energy of rising bubbles, we assume that bubble gases are released to the atmosphere immediately when the bubbles reach the lake surface during ice-free seasons. In winter, considering that the water convection associated with hotspot bubbling events could prevent ice from freezing when air temperature is higher than −15°C [*Zimov et al.*, 2001], the model is set to allow the penetration of high-intensity bubbles even when the topmost layers of lake are frozen. In contrast, ice layers are set to trap the background and other low-intensity bubbles and the gases of trapped bubbles will be reallocated into four gas pools. With the melting of ice layers in spring, 60% of CH_4 preserved in the winter CH_4 pool will eventually be liberated into the atmosphere [*Greene et al.*, 2014].

2.1.5. Modeling Dissolved Gases

Within the water column, the dissolved CH_4 can either be oxidized by oxygen (O_2) ($CH_4+2O_2=2H_2O+CO_2$) or emitted via diffusion. The existence of this aerobic reaction implies that the magnitude of CH_4 emissions can be adjusted by the abundance of dissolved O_2 and the activity of methanotrophic bacteria. The oxygenated condition in lake water can be maintained by O_2 diffusion from air and the photosynthesis of phytoplankton and macrophytes. To simplify, the production of O_2 via photosynthesis is not included in the model. We hypothesize that this simplification will just slightly downgrade the simulation of dissolved CH_4 because without photosynthesis dissolved O_2 in the epilimnion can be replenished by O_2 diffusion from the air in open-water seasons.

Thus, the overall dynamics of four gases (N_2, O_2, CO_2, and CH_4) are governed by the following 1-D diffusion equations:

$$\frac{\partial C_{N_2,w}}{\partial t}=\frac{\partial}{\partial z}\left(D_{N_2,w}\frac{\partial C_{N_2,w}}{\partial z}\right)\pm L_{N_2} \tag{20}$$

$$\frac{\partial C_{O_2,w}}{\partial t}=\frac{\partial}{\partial z}\left(D_{O_2,w}\frac{\partial C_{O_2,w}}{\partial z}\right)-2\times V_{oxid}(T)\frac{C_{O_2,w}}{k_{MM,O_2}+C_{O_2,w}}\frac{C_{CH_4,w}}{k_{MM,CH_4}+C_{CH_4,w}}\pm L_{O_2} \tag{21}$$

$$\frac{\partial C_{CO_2,w}}{\partial t}=\frac{\partial}{\partial z}\left(D_{CO_2,w}\frac{\partial C_{CO_2,w}}{\partial z}\right)+V_{oxid}(T)\frac{C_{O_2,w}}{k_{MM,O_2}+C_{O_2,w}}\frac{C_{CH_4,w}}{k_{MM,CH_4}+C_{CH_4,w}}\pm L_{CO_2} \tag{22}$$

$$\frac{\partial C_{CH_4,w}}{\partial t}=\frac{\partial}{\partial z}\left(D_{CH_4,w}\frac{\partial C_{CH_4,w}}{\partial z}\right)-V_{oxid}(T)\frac{C_{O_2,w}}{k_{MM,O_2}+C_{O_2,w}}\frac{C_{CH_4,w}}{k_{MM,CH_4}+C_{CH_4,w}}\pm L_{CH_4} \tag{23}$$

where $D_{N_2,w}$, $D_{O_2,w}$, $D_{CO_2,w}$, and $D_{CH_4,w}$ are the diffusivities of four gases in water ($m^2\ s^{-1}$), k_{MM,O_2} and k_{MM,CH_4} are the half-saturation constants of Michaelis-Menten kinetics for methanotrophic reaction ($\mu mol\ m^{-3}$), $V_{oxid}(T)$ is the oxidation potential of Michaelis-Menten reaction, and L_{N_2}, L_{O_2}, L_{CO_2}, and L_{CH_4} are the gas exchange terms defined in equation (19) ($\mu mol\ m^{-3}\ s^{-1}$). $D_{N_2,w}$, $D_{O_2,w}$, $D_{CO_2,w}$, and $D_{CH_4,w}$ are assumed to be equal to the thermal diffusivity of water. The potential rate of methanotrophy is defined as a function of water temperature [*Zhuang et al.*, 2004]:

$$V_{oxid}(T)=Q_{CH_4}\cdot OQ_{10}{}^{(T-T_{or})/10} \tag{24}$$

where Q_{CH_4} is the maximum oxidation potential when aqueous O_2 and CH_4 are not limited ($\mu mol\ m^{-3}\ s^{-1}$), OQ_{10} is a factor by which the oxidation potential increases with a 10°C rise in temperature, and T_{or} (= −5.5°C) is the oxidation reference temperature [*Zhuang et al.*, 2004].

For diffusion equations (19–22), the flux rate of gas m across the water-air interface is defined as $k_{T,m}\times\left(C_{surf,m}-X_m p_{atm}\right)$ [*Riera et al.*, 1999], where $k_{T,m}$ is the piston velocity of gas m ($m\ s^{-1}$), $C_{surf,m}$ is the concentration of dissolved gas m at the air-water interface ($\mu mol\ m^{-3}$), and X_m is the mixing ratio of gas m in the air. The piston velocity of gas m can be derived by an empirical relationship with wind speed [*Riera et al.*, 1999]:

$$k_{T,m}=2.778\times10^{-6}\times\left(2.07+0.125\times U_{10}{}^{1.7}\right)\times\left(\frac{Sc_m}{600}\right)^{0.5} \tag{25}$$

where Sc_m is the Schmidt number of gas m, and U_{10} is the wind speed at 10 m height ($m\ s^{-1}$).

At the water-sediment interface, the fluxes of O_2 and CO_2 are assumed to be zero and of CH_4 and N_2 are determined by the concentration gradients between the two mediums.

2.2. Model Implementation and Simulation

2.2.1. Numerical Techniques

All models described above are discretized firstly in the spatial domains and then advanced in the time domain with a fourth-order adaptive Runge-Kutta-Fehlberg method [*Burden et al.*, 1978]. Specifically, we use the first-order finite difference method in the z and r directions for the bubbling model and the second-order finite difference method in the z direction for the dissolved gas, CH_4 emissions, water thermal, and sediment thermal models. Although modeling bubble dynamics in lakes can better quantify CH_4 emissions from this aquatic system, a critical challenge in the attempt is to guarantee the nonnegativity of solutions in

equation (15), as bubble gas concentrations could be very small. Our numerical experiments indicate that negative solutions of the bubble model could reduce model efficiency, distort model prediction, and lead to numerical instability. To ameliorate model simulations, we incorporate a scheme described by *Shampine et al*. [2005] into the fourth-order Runge-Kutta-Fehlberg method to recursively curtail the running time step when large negative gas concentrations occur, until the negative values are small enough to assign safely as zero.

2.2.2. Data Collection

The bLake4Me model is driven with air temperature, air dew-point temperature, air pressure, wind speed, rainfall, and snow fall, all of which are extracted from a data set of European Center for Medium-Range Weather Forecasts (ECMWF) Interim reanalysis (ERA-Interim) at a $0.75^\circ \times 0.75^\circ$ resolution [*Dee and Uppala*, 2009; http://apps.ecmwf.int/datasets/data/interim_full_daily/] using the inverse of square distance as weight. The ECMWF ERA-Interim reanalysis data set provides those parameters at a 12 h scale from 1 January 1979 to 31 July 2013. The density of catchment soil organic carbon is extracted from a $0.05^\circ \times 0.05^\circ$ static soil organic carbon map of the Northern Circumpolar Soil Carbon Database version 2 (NCSCDv2) [*Hugelius et al*., 2013] also using the inverse of square distance as weight.

We evaluated the bLake4Me modeling framework at five small lake sites in Siberia and Alaska (Table 1): two thermokarst lakes formed in late Pleistocene-aged yedoma permafrost in the Kolyma River Basin of northeastern Siberia (Shuchi Lake and Tube Dispenser Lake), one yedoma-type thermokarst lake in the Tanana River Basin of Alaska (Goldstream Lake), one yedoma-type thermokarst lake in the continuous permafrost zone of the northern Seward Peninsula, Alaska (Claudi Lake) and one kettle lake in the continuous permafrost region (nonyedoma and nonthermokarst) of northern Alaska (Toolik Lake). Here we refer to "a small lake" as a lake with area smaller than 2 km^2 and "a deep lake" as a lake with depth deeper than 20 m. The field data set includes daily water and sediment temperature from Goldstream Lake, water temperature, and CH_4 concentration profiles from Shuchi Lake and Tube Dispenser Lake, and background ebullition, point-source seep ebullition and hotspot seep ebullition fluxes from both thermokarst and nonthermokarst sites of five lakes (Table 1). The boundary conditions (air temperature, snow cover, and wind speed) to drive model simulations for these lakes are presented in supporting information Figures S1–S4.

CH_4 ebullition fluxes were measured at the validation lakes following methods described and employed on these by *Walter et al*. [2006, 2008], *Walter Anthony et al*. [2010], and *Walter Anthony and Anthony* [2013]. Briefly, we estimated seep and nonseep (background) ebullition separately. Seeps are defined as point-source locations of repeated bubbling and identified by the appearance of trapped bubbles in ice as Type A ("kotenok")—stacks of small individual bubbles, Type B ("koshka")—bubbles clustered in multiple ice layers, Type C ("kotara")—single large pockets of near 100% merged bubbles stacked in ice, and hotspot—ice-free hole in lake ice due to frequent bubbling.

To quantify seep ebullition, we removed snow from early winter lake ice to expose ebullition bubble clusters trapped in ice for seep classification, GPS mapping, flux measurements, and gas collection using submerged bubble traps. On foot, we surveyed all individual seeps within 6–12 1 m $\times$ 50 m plots per lake. Plots were positioned randomly within both littoral and profundal zones of lakes. Ice was opened above a subset of the seeps in each lake for placement of submerged bubble traps over the seeps. Manual [*Walter et al*., 2006, 2008] or semiautomated [*Walter Anthony et al*., 2010] bubble traps remained in place over individual seeps year round, providing daily and seasonal flux from sediment data for individual seeps. Seep class-specific flux rates and bubble CH_4 and N_2 concentrations measured on a subset of seeps were applied to the density of all mapped seeps in different littoral and profundal zones of the lakes to estimate whole-lake ebullition rates from sediments, indexed by Julian Day of the year.

Thirty day averages of bubbling rates (mL gas $seep^{-1}$ d^{-1}) indexed by Julian Day of the year were determined through bubble-trap measurements of seep fluxes and associated with seep classes for each Julian Day of the year [*Walter Anthony et al*., 2010]. This data set consists of $\sim$210,000 individual flux measurements made using submerged bubble traps placed over ebullition seeps year round. These class-specific fluxes were applied to the whole-lake mean densities of seeps on lakes to derive estimates of bubble-release rates from lakes indexed by Julian Day. To determine mass-based estimates of CH_4 and CO_2 in ebullition bubbles, we applied lake-specific measurements of CH_4 and CO_2 bubble concentrations to the individual lakes where seep-bubble gases were collected and measured. Methods of bubble-trap gas collection

and measurements were described in detail by *Walter et al*. [2008]. We sampled with bubble traps and measured by gas chromatography the CH_4 and CO_2 compositions of seep ebullition bubbles collected from up to 246 individual ebullition events per lake. In Toolik Lake and Lake Claudi, where no or few seep-bubble gas concentrations were determined, we applied mean values of CH_4% by seep class [*Walter Anthony et al*., 2010] A, 73%; B, 75%; C, 76%; hotspot, 78%. Whole-lake mean ebullition was the sum of seep fluxes observed along transects divided by the total area surveyed in each lake. In a recent comparison of methods for quantifying ebullition, *Walter Anthony and Anthony* [2013] showed that when at least three 50 m transects per lake are used to quantify seep ebullition, the estimate of mean whole-lake ebullition is 4–5 times more accurate than the mean flux determined by placement of seventeen 0.2 m^2 bubble traps randomly distributed across lake surfaces.

In the Siberian lakes, Lake Shuchi and Lake Tube Dispenser, we also estimated background ebullition in different thermokarst margin, nonthermokarst margin, and lake center zones of the lakes as the average ebullition fluxes observed in randomly placed traps within these zones [*Walter et al*., 2006]. In *Walter et al*. [2006], random placement of up to 14 traps per lake with continuous, year-round monitoring revealed that this "background" bubbling accounted for 24 ± 6% of the total emissions. We included the estimated flux from background ebullition in addition to point-source seeps because the probability of capturing point-source seeps in randomly placed traps was 0.001% and there was no overlap between values of point-source fluxes and values of background ebullition.

Diffusive flux at Shuchi and Tube Dispenser lakes, determined by *Walter et al*. [2006], was estimated from biweekly surface water concentrations of CH_4 measured during the ice-free summer period in the lake center at Shuchi and Tube Dispenser lakes (mg CH_4 m^{-2} yr^{-1}) following methodology of *Kling et al*. [1992].

2.3. Model Sensitivity to Parameters

As model parameters can vary in very broad ranges [*Segers*, 1998; *Walter and Heimann*, 2000; *Tang and Zhuang*, 2009], it is essential to first evaluate model sensitivity to parameters. Two index values for each parameter are evaluated, including first-order sensitivity index (FOSI) and total-order sensitivity index (TOSI) [*Sobol'*, 1993; *Sobol'*, 2001]. The first-order index is defined as the reduction of model output variance when the assessed parameter is fixed. The total-order index is defined as the reduction of model output variance when all other parameters except the assessed parameter are fixed [*Sobol'*, 1993]. We employ a negativity-free scheme described in detail by *Saltelli* [2002] and Monte Carlo ensemble simulations (MC) to calculate those FOSI and TOSI indices. The uncertainties of FOSI and TOSI indices are estimated by using the bootstrap method [*Davison and Hinkley*, 1997].

Fourteen parameters in Table 2 are tested at the 1.7 m deep thermokarst margin of Shuchi Lake from 28 April 2003 to 30 June 2004 by comparing the simulated daily mean CH_4 ebullition fluxes. These parameters are assumed to be uniformly distributed with ranges documented in Table 2.

2.4. Model Calibration

Since many parameters listed in Table 2 are hard to measure, we employ a global parameterization scheme, the Shuffled Complex Evolution (SCE-UA) method, developed by *Duan et al*. [1994] to constrain their values. The SCE-UA method includes the following steps: (1) sample s points (parameter set) in parameter space and run one simulation with each parameter set; (2) sort the s points in order of ascending mean square root of model-simulation difference (DRMS) (the goal is to minimize DRMS); (3) partition the s points into p complexes, each contains m points. The partition principle is that the complex i contains every $p(k-1)+i$ ranked point, where $k = 1, 2, \ldots, m$; (4) evolve each complex according to the competitive complex evolution (CCE) algorithm, which was modified from the Nelder-Mead method; (5) merge the points of all evolved complexes into a single sample population (new sample); and (6) check convergence, stop if the minimum DRMS has been smaller than the criteria or the whole population shrinks to a single point; otherwise continue with step (2). The optimum values of the number of sampling points s, the number of complexes p and the number of points in each complex m have been identified by *Duan et al*. [1994].

In the model, instead of calibrating all parameters together with a single data set, we partition them into three categories: temperature-, methanotrophy-, and methanogenesis-sensitive (denoted as "T-sen," "Mo-sen," and "Mp-sen," respectively) parameters. The parameters of each category are evaluated separately with the observed lake water and sediment temperature, CH_4 concentrations, and CH_4 emissions.

Table 2. Model Parameters Involved in the Sensitivity Analysis[a]

		Thermokarst		Nonthermokarst		
Parameter	Prior Range	FOSI	TOSI	FOSI	TOSI	References
k_{solid}	[0.25, 2.9]	$3.7 \times 10^{-5} \pm 2.9 \times 10^{-6}$	$0.0134 \pm 1.3 \times 10^{-5}$	$7.1 \times 10^{-6} \pm 1.1 \times 10^{-6}$	$0.0014 \pm 1.7 \times 10^{-6}$	*Hillel* [1980] and *Johnston* [1939]
c_{ps}	[750, 1930]	$2.8 \times 10^{-4} \pm 2.0 \times 10^{-6}$	$0.0103 \pm 1.2 \times 10^{-5}$	$3.7 \times 10^{-4} \pm 2.1 \times 10^{-6}$	$0.0026 \pm 2.1 \times 10^{-6}$	*Hillel* [1980] and *Johnston* [1939]
Π	[30, 60]	$6.2 \times 10^{-4} \pm 2.8 \times 10^{-6}$	$0.0145 \pm 1.3 \times 10^{-5}$	$6.2 \times 10^{-5} \pm 7.5 \times 10^{-7}$	$3.0 \times 10^{-4} \pm 9.0 \times 10^{-7}$	*Hillel* [1980]
ρ_s	[1500, 2700]	$1.9 \times 10^{-4} \pm 7.9 \times 10^{-7}$	$0.0044 \pm 6.2 \times 10^{-6}$	$2.3 \times 10^{-5} \pm 3.2 \times 10^{-7}$	$1.1 \times 10^{-4} \pm 3.3 \times 10^{-7}$	*Hillel* [1980] and *Donahue et al.* [1983]
OQ_{10}	[1.4, 3.5]	$2.3 \times 10^{-4} \pm 7.7 \times 10^{-7}$	$0.0011 \pm 5.3 \times 10^{-6}$	$3.5 \times 10^{-5} \pm 6.1 \times 10^{-7}$	$1.1 \times 10^{-4} \pm 3.4 \times 10^{-7}$	*Tang and Zhuang* [2009]
Q_{CH_4}	[0.1, 100]	$8.2 \times 10^{-5} \pm 1.4 \times 10^{-6}$	$0.0027 \pm 5.2 \times 10^{-6}$	$1.9 \times 10^{-4} \pm 1.5 \times 10^{-6}$	$2.8 \times 10^{-4} \pm 8.8 \times 10^{-7}$	*Segers* [1998]
k_{MM,CH_4}	[1, 66.2]	$1.6 \times 10^{-4} \pm 1.6 \times 10^{-6}$	$0.0017 \pm 5.7 \times 10^{-6}$	$7.0 \times 1\,0^{-5} \pm 8.7 \times 10^{-7}$	$1.0 \times 10^{-4} \pm 3.3 \times 10^{-7}$	*Segers* [1998]
k_{MM,O_2}	[1, 200]	$3.1 \times 10^{-4} \pm 8.5 \times 10^{-7}$	$0.0019 \pm 5.6 \times 10^{-6}$	$2.7 \times 10^{-4} \pm 1.5 \times 10^{-6}$	$3.4 \times 10^{-4} \pm 1.0 \times 10^{-6}$	*Segers* [1998] and *van Bodegom et al.* [2001]
$PQ_{10,new}$	[1.7, 16]	$0.0141 \pm 1.7 \times 10^{-5}$	$0.0638 \pm 2.1 \times 10^{-5}$	$0.1346 \pm 1.0 \times 10^{-4}$	$0.4748 \pm 8.2 \times 10^{-5}$	*Walter and Heimann* [2000]
$R_{c,new}$	[0.002, 0.02]	$0.0216 \pm 2.4 \times 10^{-5}$	$0.0845 \pm 3.2 \times 10^{-5}$	$0.4551 \pm 2.9 \times 10^{-4}$	$0.8154 \pm 5.2 \times 10^{-5}$	*Kessler et al.* [2012]
α_H	[1.0, 10.0]	$0.0036 \pm 1.9 \times 10^{-5}$	$0.0227 \pm 1.6 \times 10^{-5}$	$0.0270 \pm 2.8 \times 10^{-5}$	$0.1857 \pm 1.2 \times 10^{-4}$	*Stepanenko et al.* [2011]
c_e	[29.5, 407]	$4.1 \times 10^{-5} \pm 2.6 \times 10^{-7}$	$9.7 \times 10^{-4} \pm 9.0 \times 10^{-7}$	$2.0 \times 10^{-5} \pm 2.8 \times 10^{-7}$	$3.5 \times 10^{-5} \pm 2.6 \times 10^{-7}$	*Algar and Boudreau* [2009]
$PQ_{10,old}$	[1.0, 3.6]	$0.0067 \pm 7.5 \times 10^{-6}$	$0.0273 \pm 1.5 \times 10^{-5}$	$2.2 \times 10^{-6} \pm 1.1 \times 10^{-7}$	$6.1 \times 10^{-6} \pm 7.9 \times 10^{-8}$	*Segers* [1998]
$R_{c,old}$	[0.002, 0.02]	$0.9089 \pm 6.2 \times 10^{-5}$	$1.5215 \pm 1.3 \times 10^{-4}$	$3.6 \times 10^{-7} \pm 1.4 \times 10^{-7}$	$1.3 \times 10^{-5} \pm 9.5 \times 10^{-8}$	*Kessler et al.* [2012]

[a]Parameter units: k_{solid} (W m^{-1} K^{-1}); c_{ps} (J kg^{-1} K^{-1}); Π (%); ρ_s (kg m^{-3}); OQ_{10} (n/a); Q_{CH_4} (μmol m^{-3} s^{-1}); k_{MM,CH_4} (mmol m^{-3}); k_{MM,O_2} (mmol m^{-3}); $PQ_{10,new}$ (n/a); $R_{c,new}$ (yr^{-1}); α_H (m^{-1}); c_e (hr^{-1}); $PQ_{10,old}$ (n/a); and $R_{c,old}$ (yr^{-1}).

Specifically, the "T-sen" parameters are calibrated with the observed temperature at a 2.3 m deep nonthermokarst area of Goldstream Lake. The "Mo-sen" parameters are calibrated with the observed dissolved CH_4 profiles at an 11 m deep center of Shuchi Lake. The "Mp-sen" parameters are divided further for four subgroups: the ^{14}C-depleted carbon pool, the ^{14}C-enriched carbon pool of thermokarst margins, the ^{14}C-enriched carbon pool of nonthermokarst margins, and the ^{14}C-enriched carbon pool of lake centers. The "Mp-sen" parameters for the ^{14}C-depleted and the ^{14}C-enriched carbon pools at thermokarst margins are calibrated with the background and seep ebullition fluxes measured from the thermokarst margins of Shuchi Lake with a mean depth of 4 m. The "Mp-sen" parameters for the ^{14}C-enriched carbon pool at nonthermokarst margins are calibrated with the background ebullition fluxes measured from the nonthermokarst margins of Shuchi Lake with a mean depth of 3 m. The "Mp-sen" parameters of the ^{14}C-enriched carbon pool at lake centers are calibrated with the background ebullition fluxes measured from the centers of Shuchi Lake with a mean depth of 8 m. The multiplier α_{erode} is calibrated with the CH_4 background ebullition fluxes measured from the thermokarst margins with a mean depth of 4 m and the nonthermokarst margins with a mean depth of 3 m at Shuchi Lake together. The calibrated "T-sen" and "Mo-sen" parameters are applied to all sites or zones of the five studied lakes. The calibrated "Mp-sen" parameters of each subgroup are only applied to the corresponding lake zones. To reduce the simulation error due to seep flux heterogeneity over small (<10 m) spatial scales [*Walter Anthony and Anthony*, 2013], CH_4 fluxes are modeled for a lake zone with the use of mean water depth and lake bottom temperature.

3. Results and Discussion

3.1. Parameter Sensitivity Analysis

From Table 2, the tested parameters can be allocated into three categories: sensitive parameters for CH_4 ebullition fluxes (with FOSI $\geq$ 5% or TOSI $\geq$ 5%), insensitive parameters for CH_4 ebullition fluxes (with FOSI $\leq$ 1% and TOSI $\leq$ 1%), and other weakly sensitive parameters (with 1% $\leq$ FOSI $\leq$ 5% and 1% $\leq$ TOSI $\leq$ 5%). Noticeably, both seep and background CH_4 fluxes are susceptible to parameters related to substrate availability of methanogenesis ($R_{c,\ new}$ and $R_{c,\ old}$). This close correlation between methanogenetic magnitude and available carbon pool size implies that the thawing permafrost is likely to fuel carbon transfer from lakes sediments to the earth atmosphere. In addition to substrate availability, the parameters relevant to the thermal response of methanogenesis ($PQ_{10,\ new}$ and α_H) can also influence background emissions significantly. The sensitivity of seep emissions to temperature ($PQ_{10,\ old}$) is relatively small as the ^{14}C-depleted carbon pool is within cold deep sediments.

CH_4 ebullition fluxes are found less susceptible to methanotrophy-related parameters (OQ_{10}, Q_{CH_4}, k_{MM,CH_4}, and k_{MM,O_2}) because the relatively short residence time of bubbles in high-intensity ebullition could limit CH_4 dissolution. But the total CH_4 fluxes in nonthermokarst lakes where diffusive fluxes are relatively large can still be sensitive to methanotrophy-related parameters because much of diffused CH_4 can be oxidized in the water column. Ebullition is also found insensitive to some soil characteristics (k_{solid}, c_{ps}, Π, and ρ_s). It is likely that the thawing of permafrost is a slow and long-term process and its dependence on soil properties cannot be assessed in a 2 year simulation. Our model shows that owing to the low gas diffusivity in sediments, produced CH_4 is prone to accumulate locally, yielding bubbles rather than diffusing from sediments to the water column. As the produced CH_4 is not able to transport to other layers quickly and the bubble formation rate and pore-water CH_4 concentrations are negatively correlated, a lower c_e in equation (14) will be compensated by the corresponding higher CH_4 gradient, making the ebullition rates with different c_e comparable. Thus, as shown in Table 2, the parameter c_e has small FOSI and TOSI indices.

3.2. Site-level Model Experiments

3.2.1. Shuchi Lake

Figures 2 and 3 show a comparison of model simulations to observations on water temperature, CH_4 concentrations, and ebullition fluxes at Shuchi Lake, Siberia in 2003. The temperature profiles of the water column were recorded at the 11 m deep lake center in both ice-cover (1 May and 28 May) and ice-free days (14 June, 30 June, 14 July,/28 July, 9 August, 9 September, and 1 October). As shown in Figure 2, the model reproduced the observed temperature profiles at most of the water layers with mean error less than 1°C (0.8°C for 1 May, 0.69°C for 28 May, 0.75°C for 14 June, 0.8°C for 30 June, 0.95°C for 14 July, 0.42°C for 28 July, 1.1°C for 9 August, 0.77°C for 9 September, and 1.22°C for 1 October). The position of thermocline zone was also accurately simulated in most of days. The model performed the best at the hypolimnion with

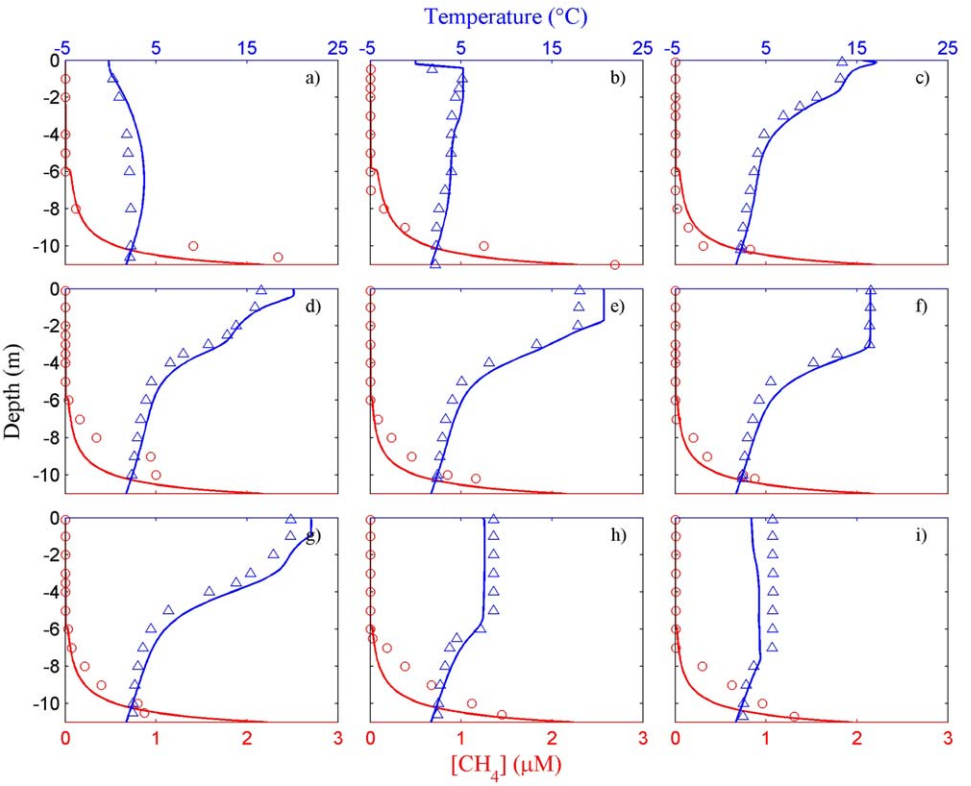

Figure 2. Comparison of the simulated (blue line) and observed (blue triangle) temperature profiles and comparison of the simulated (red line) and observed (red circle) CH_4 concentration profiles at the 11 m deep center of Shuchi Lake in following days: (a) 1 January 2003; (b) 28 May 2003; (c) 14 June 2003; (d) 30 June 2003; (e) 14 July 2003; (f) 28 July 2003; (g) 9 August 2003; (h) 9 September 2003; and (i) 1 October 2003.

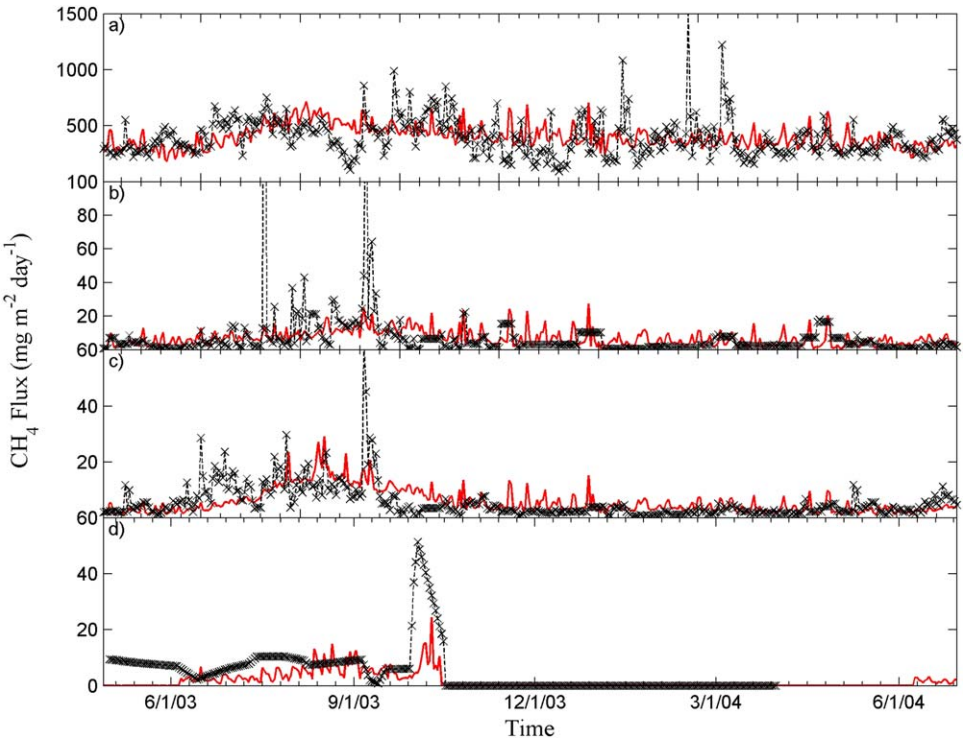

Figure 3. Comparison of the simulated and observed CH_4 fluxes at Shuchi Lake, Siberia on (a) CH_4 ebullition fluxes from the thermokarst margin zone SC-TKM; (b) CH_4 ebullition fluxes from the nonthermokarst margin zone SC-NTKM; (c) CH_4 ebullition fluxes from the lake center zone SC-CT; and (d) CH_4 diffusive fluxes from SC-CT. Ebullition fluxes include ebullition from point-source seeps and nonpoint-source background bubbling. Note different scales on the *Y* axis.

an average deviation of 0.37°C and the worst at the epilimnion with an average deviation of 1.51°C. This performance inhomogeneity reveals the inaptitude of our simple energy balance and water overturning schemes in defining the strong exchange of energy and momentum occurring near to the water surface. However, the high accuracy of temperature simulations achieved in the hypolimnion, including the stable 2.5°C water temperature at the lake bottom, is believed to furnish credible climatic driving of sediment methanogenesis. As indicated in Figures 2a and 2b, the model performed well in simulating the ice season duration of Shuchi Lake.

The dissolved CH_4 concentration ($[CH_4]$) profiles shown in Figure 2 were also modeled and recorded at the 11 m deep lake center in the above days. Our model results suggest that dissolved CH_4 in the water column during summer originates primarily from surface sediment methanogenesis (99%), and secondarily from bubble dissolution (1%). The mean error of simulations is 0.26 μM (1 $\mu M = 10^{-3}$ mole m^{-3}) for 1 May, 0.1 μM for 28 May, 0.05 μM for 14 June, 0.12 μM for 30 June, 0.06 μM for 14 July, 0.05 μM for 28 July, 0.05 μM for 9 August, 0.13 μM for 9 September, and 0.12 μM for 1 October. Despite the high absolute errors in deep waters, the relative errors are the highest in layers near to the water surface, as the gas dissolution from breaking bubbles at surface is not fully modeled.

Figure 3 compares the simulated and observed CH_4 ebullition or diffusive fluxes from Shuchi Lake at a thermokarst margin zone with a mean depth of 4 m ("SC-TKM"), a nonthermokarst margin zone with a mean depth of 3 m ("SC-NTKM"), and a nonthermokarst center with a mean depth of 8 m ("SC-CT") from 28 April 2003 to 30 June 2004. Our data suggest that relative to kotara and hotspot ebullition, background, kotenok, and koshka ebullition have weaker flux rates but stronger positive correlation to summer heat pulse. For instance, at the SC-NTKM and SC-CT zones where background, kotenok, and koshka ebullition dominated, pronounced emission climax occurred about 1 month after the warmest day in each year when heat pulse reached the top of sediment layers (Figures 3b and 3c). In contrast, at the SC-TKM zone, heat input only increased CH_4 emissions slightly in August (Figure 3a).

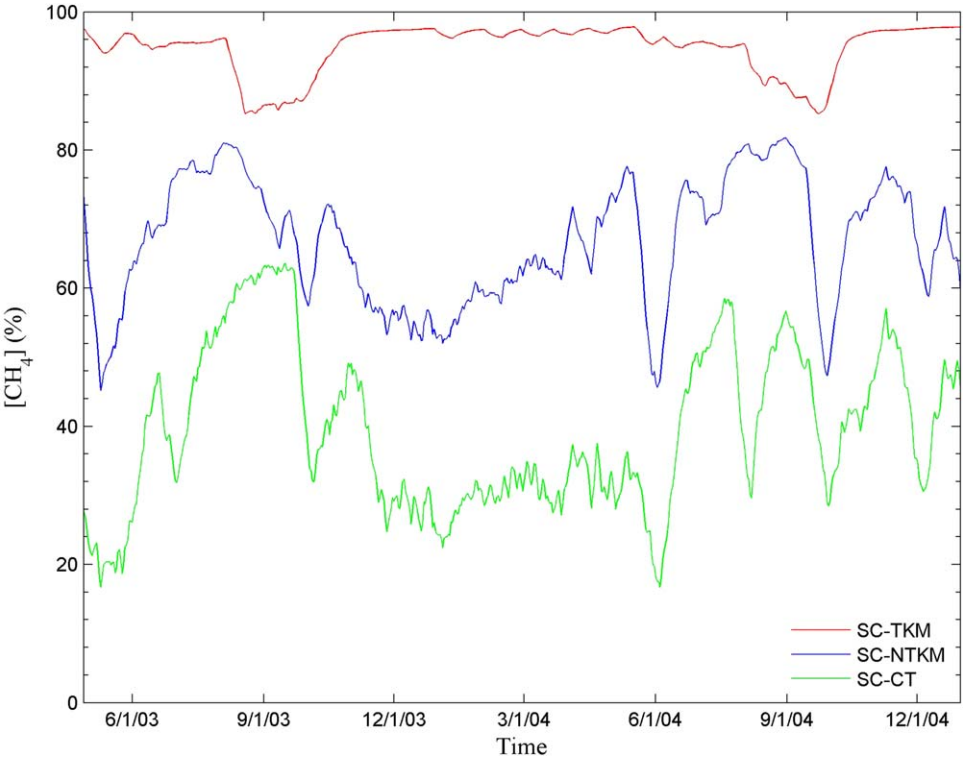

Figure 4. The variability of modeled CH_4 percentage concentrations in bubbles released from Shuchi Lake, Siberia from 28 April 2003 to 31 December 2004 (for yedoma lakes, the measured CH_4% was from 73% to 90% at thermokarst margins and 63.8 ± 16.1% in other areas).

Unlike the SC-NTKM and SC-CT zones, ebullition at the SC-TKM zone maintained high rates throughout the year, in spite of varied air temperature. The seasonal stability of CH_4 fluxes in thermokarst margins can be explained by either the small methanogenetic Q_{10} values (close to one) of the ^{14}C-depleted carbon pool [*Zimov et al.*, 1997; *Walter et al.*, 2008] or the resistance of deep sediments where the kotara and hotspot ebullition originated to heat pulse. In addition to the emission maximum observed in August, field-observed CH_4 emissions from the SC-TKM zone also peaked in October, but this was not reproduced by our model. This October maximum cannot be solely attributed to the transport of heat pulse to deeper sediment layers because with the attenuation of heat pulse in downward transport, the temperature of deep sediments in October was still much lower than that of shallow sediments in July. Alternatively, the vertical inhomogeneity of carbon content throughout yedoma permafrost is a possible cause. The mean daily error of simulated ebullition fluxes is 115.8 mg CH_4 m^{-2} d^{-1} for the SC-TKM zone, 6.2 mg CH_4 m^{-2} d^{-1} for the SC-NTKM zone, and 3.3 mg CH_4 m^{-2} d^{-1} for the SC-CT zone. As shown in Figure 3, the daily variability of observed emissions (driven by hydrostatic pressure dynamics) is the main source of errors presented above. When smoothing both observations and simulations by a 2 week moving average filter, the mean daily error of the SC-TKM simulations can be reduced significantly to 48.9 mg CH_4 m^{-2} d^{-1}. The poor representation of daily variability in ebullition is likely a result of using the global-scale climate data set to drive the model instead of station measurements. However, this problem could also be caused by the deterministic structure of our model. As argued by *Coulthard et al.* [2009], modeling a stochastic bubble release process with deterministic equations is questionable. Previous studies demonstrated that ebullition is a dominant way of transporting CH_4 from arctic lakes: on a whole-lake basis, most of the time over 90% of CH_4 was released via ebullition and less than 10% was via diffusion [*Walter et al.*, 2006; *Walter Anthony et al.*, 2010]. Most of our simulations except in lake centers endorse this claim. In the lake centers, such as the SC-CT zone presented in Figure 3d, the diffusive fluxes can be comparable to the zone's ebullition fluxes.

Figure 4 shows the variability of simulated bubble CH_4 percentage concentration (CH_4%) calculated at the lake surface from 28 April 2003 to 31 December 2004. *Walter Anthony et al.* [2010] previously observed that

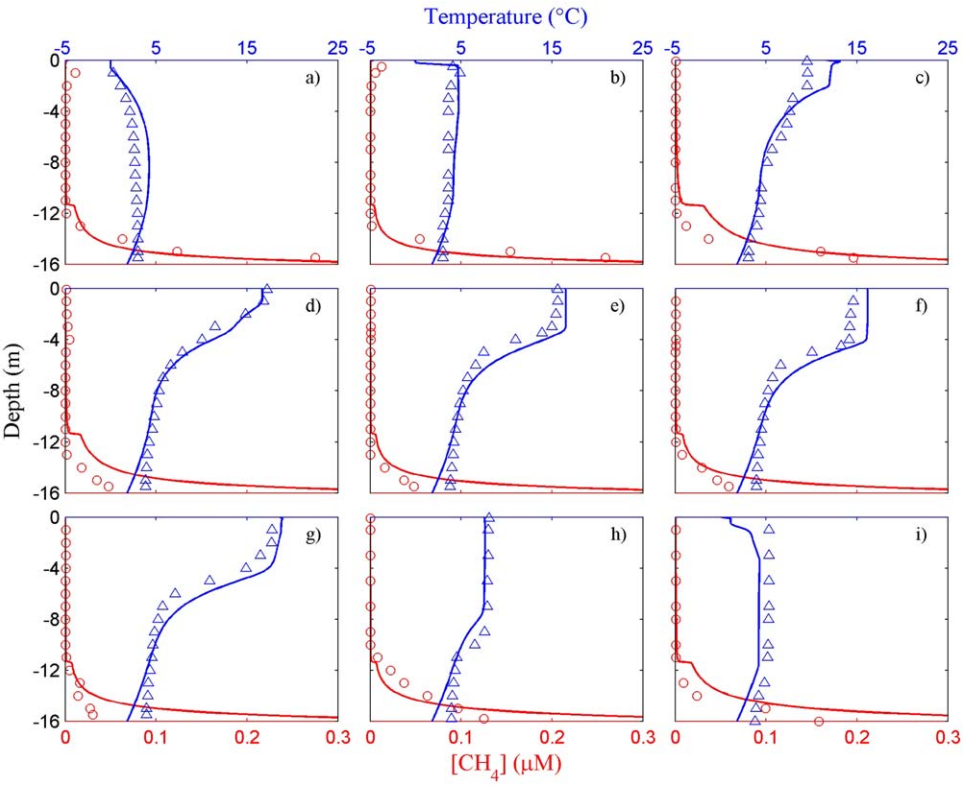

Figure 5. Comparison of the simulated (blue line) and observed (blue triangle) temperature profiles and comparison of the simulated (red line) and observed (red circle) CH_4 concentration profiles at the 16 m deep center of Tube Dispenser Lake in following days: (a) 3 May 2003; (b) 30 May 2003; (c) 16 June 2003; (d) 2 July 2003; (e) 16 July 2003; (f) 31 July 2003; (g) 11 August 2003; (h) 13 September 2003; and (i) 3 October 2003.

CH_4 content in bubbles (%) varied significantly in different seep types across yedoma and nonyedoma panarctic lakes (kotenok: 73%; koshka: 75%; kotara: 76%; hotspot: 78%). In yedoma lakes, CH_4% in seep bubbles tends to be higher than in nonyedoma lakes. For instance, *Walter Anthony and Anthony* [2013] reported the following mean seep class CH_4% concentrations in Goldstream Lake: (kotenok = 82 ± 3%, n = 6; koshka = 83 ± 7%, n = 3; kotara = 85 ± 1%, n = 14; hotspot = 89 ± 1%, n = 19; reported as mean ± standard error, *n* is the number of seeps). *Walter et al.* [2008] further argued that the strong negative correlation between CH_4/N_2 bubble concentration ratios and ebullition flux rates indicated that atmospheric N_2 diffusion was too slow to replenish N_2 loss during bubble formation (process termed N_2 stripping) [*Chanton et al.*, 1989]. As a result, more CH_4 rather than N_2 resided in bubbles forming in high-flux seeps [*Walter et al.*, 2008]. The high CH_4% at the SC-TKM zone implies that it is a plausible argument. The results of the SC-TKM, SC-NTKM, and SC-CT zones suggest that ebullition rate is the foremost control factor of CH_4% (64%), and when ebullition rate is low lake depth is also an important control factor (16%). Another pattern shown in Figure 4 is the negative seasonal correlation between thermokarst and nonthermokarst areas on bubble CH_4 concentration. For nonthermokarst areas, the peak of ebullition fluxes in summer corresponded to the depleting of sediment N_2 and the increase of CH_4 concentration in bubbles. For thermokarst zones, where the ebullition rate was very high, heat input did not change the CH_4/N_2 ratio noticeably. In winter, ice layers can curtail bubble transport distance in the water column, causing the gas loss of rising bubbles due to dissolution to be reduced (20%). The simulated CH_4% is 91 ± 6% for the SC-TKM zone, 63 ± 18% for the SC-NTKM zone, and 40 ± 23% for the SC-CT zone. Previously, *Walter et al.* [2008] observed that bubbles from background ebullition contained 63.8 ± 16.1% CH_4. The relatively low CH_4% in the modeled lake-center bubbles here may be explained by CH_4 production in the surface sediments, where pore water N_2, replenished through gas diffusion from the water column, is much higher than in the deeper underlying sediments. In addition, the overestimation of bubble N_2 content fractions in Figure 4 could also partly be

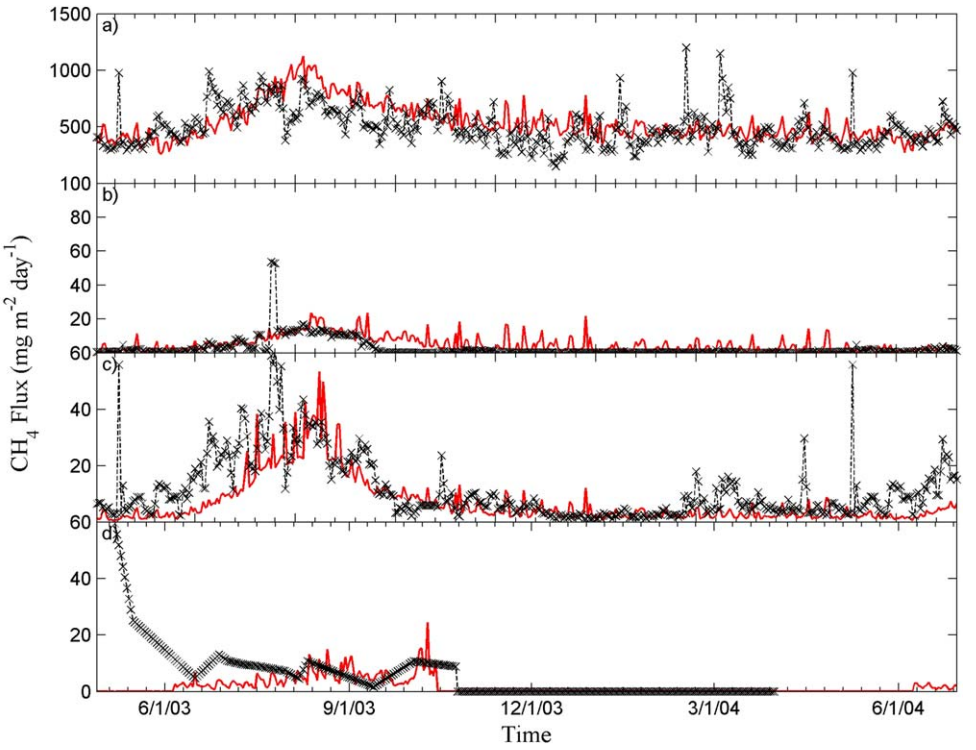

Figure 6. Comparison of the simulated and observed CH_4 fluxes at Tube Dispenser Lake, Siberia on (a) CH_4 ebullition fluxes from the thermokarst margin zone TD-TKM; (b) CH_4 ebullition fluxes from the nonthermokarst margin zone TD-NTKM; (c) CH_4 ebullition fluxes from the lake center zone TD-CT; and (d) CH_4 diffusive fluxes from TD-CT. Ebullition fluxes include ebullition from point-source seeps and nonpoint-source background bubbling. Note different scales on the *Y* axis.

explained by the missing terms of N_2 sinks in the water and sediment columns, e.g., possible N_2 fixation reactions [*Torrey and Lee*, 1976].

3.2.2. Tube Dispenser Lake

Figures 5 and 6 show a comparison of model simulations to observations on water temperature, CH_4 concentrations, and ebullition fluxes at Tube Dispenser Lake, Siberia in 2003. Figure 5 presents the water temperature observations recorded at the 16 m deep lake center in both ice-cover (3 May and 30 May) and ice-free days (16 June, 2 July, 16 July, 31 July, 11 August, 13 September and 3 October). The mean errors of simulated temperature are 1.29°C in the epilimnion and 0.86°C in the hypolimnion. The underestimated lake bottom temperatures in Figure 5 could be caused by miss-incorporating the effect of bottom currents produced by basin-scale seiching in the diffusivity equation [*Wüest et al*., 2000]. For the thermocline zone, the simulation error of Tube Dispenser Lake is almost twofold larger than of Shuchi Lake (1.55°C versus 0.81°C), reflecting the complexity of water vertical mixing in high-latitude lakes. Generally as located in the same region, the two lakes exhibited similar thermal characteristics: stable stratification in the summer, minor temperature variation in the hypolimnion, and strong water mixing in the late spring and fall.

As shown in Figure 5, the bottom [CH_4] at the center of Tube Dispenser Lake was just 10 January to 5 January of [CH_4] at Shuchi Lake. This difference is likely a result of weaker gas diffusivity in the relatively deeper, larger center of Tube Dispenser Lake. In addition, since the water of Tube Dispenser Lake was warmer (bottom 4°C) and oxidation is more sensitive to temperature than CH_4 production below 15°C [*Schulz et al*., 1997; *Whalen et al*., 1990], it is possible that CH_4 oxidation was relatively higher in Tube Dispenser Lake than in Shuchi Lake. As the simulations at Shuchi Lake, our model reproduced CH_4 profiles at Tube Dispenser Lake with low deviations: 0.012 μM for 3 May, 0.015 μM for 30 May, 0.013 μM for 16 June, 0.021 μM for 2 July, 0.014 μM for 16 July, 0.014 μM for 31 July, 0.018 μM for 11 August, 0.027 μM for 13 September, and 0.054 μM for 3 October. There are two visible similarities between the two Siberian lakes regarding CH_4 concentrations and emissions. First, most of the dissolved CH_4 in both lakes is depleted within layers from the

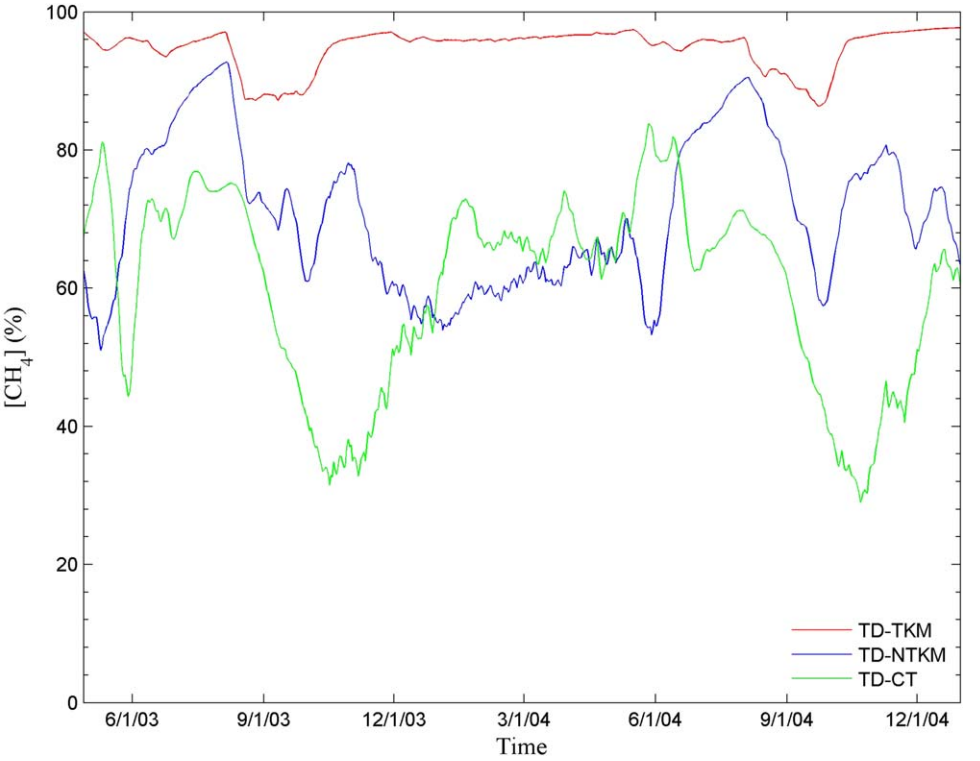

Figure 7. The variability of modeled CH_4 percentage concentrations in bubbles released from Tube Dispenser Lake, Siberia from 28 April 2003 to 31 December 2004 (for yedoma lakes, the measured CH_4% was from 73% to 90% at thermokarst margins and 63.8 ± 16.1% in other areas).

bottom of epilimnion to the top of hypolimnion because beneath the oxycline O_2 is consumed rapidly by heterotrophic respiration. Second, the ebullition in both lakes is at least an order of magnitude higher along the thermokarst margin than in the rest of the lake. This suggests that while dissolved CH_4 originating from the ^{14}C-enriched surface sediments may differ between the lakes based on different lacustrine characteristics; the ebullition dynamics, which are governed by spatiotemporal patterns of talik expansion (and associated methanogenesis from the ^{14}C-depleted thawing permafrost organic matter), are the same.

Figure 6 compares the simulated CH_4 ebullition and diffusive fluxes from Tube Dispenser Lake to observations at a thermokarst margin zone with a mean depth of 4 m ("TD-TKM"), a nonthermokarst margin zone with a mean depth of 4 m ("TD-NTKM"), and a nonthermokarst center zone with a mean depth of 12 m ("TD-CT") from 28 April 2003 to 30 June 2004. The mean daily error of simulated ebullition fluxes is 120.3 mg CH_4 m^{-2} d^{-1} for the TD-TKM zone, 3.3 mg CH_4 m^{-2} d^{-1} for the TD-NTKM zone, and 6.0 mg CH_4 m^{-2} d^{-1} for the TD-CT zone. As illustrated in section 3.2.1, the errors were mainly produced by the poor representation of daily variability of ebullition fluxes due to the coarse resolution of climate data set. If the long-term CH_4 cycle between lake system and atmosphere is the primary interest, our model tends to have credible performance. Different from the SC-TKM zone, the October maximum of ebullition fluxes was absent at the TD-TKM zone. Figures 3d and 6d both indicate that our model failed to reproduce high diffusive fluxes from lake centers prior to June. We suspect that the gas collection method used in this study is possibly responsible for the discrepancy between the model simulations and observations. In the model, Tube Dispenser Lake was still covered by ice in May or late April and assumed not to emit any gas via diffusion. It is conceivable that gas diffusion occurs through cracks of attenuated ice layers or the open holes of seeps [*Greene et al*., 2014]. A linear regression of CH_4 ebullition fluxes for the two Siberian lakes is presented in supporting information Figure S5. As shown in Figures 3 and 6, the modeled and measured CH_4 ebullition fluxes are more consistent in seasonal variability than in diurnal variability (relatively low R^2), the latter of which is largely controlled by the variability of hydrostatic pressure [*Walter Anthony et al*., 2010; *Varadharajan and Hemond*, 2012].

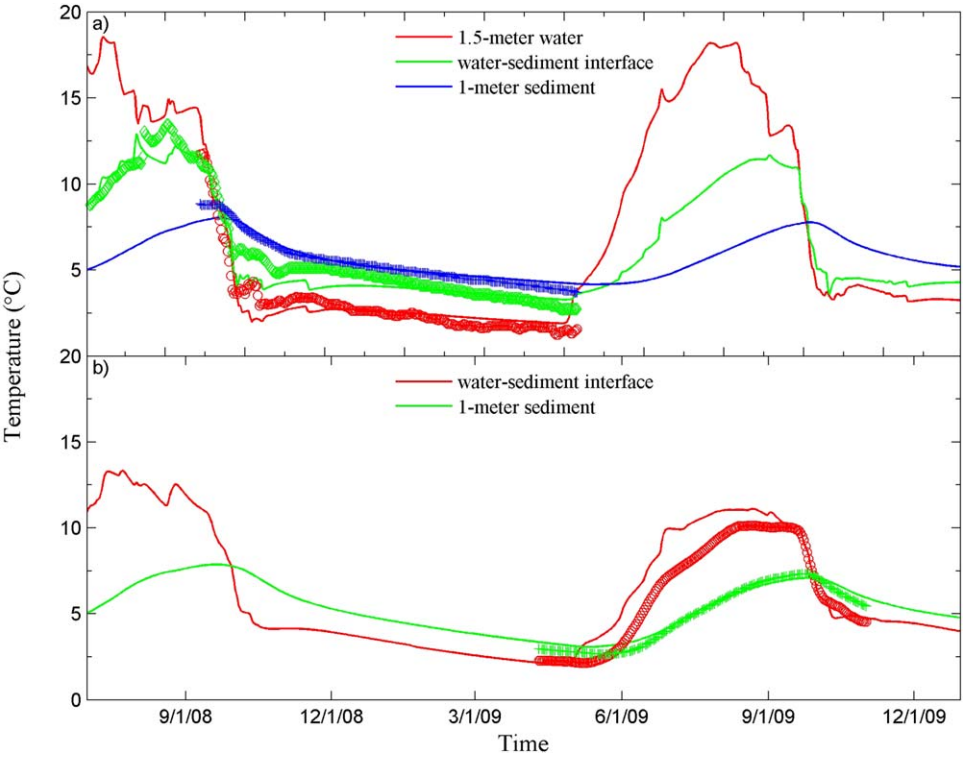

Figure 8. Comparison of the simulated (solid lines) and observed (symbols) temperatures at Goldstream Lake, Alaska (For the 2.3 m deep nonthermokarst lake center, temperatures were recorded from 3 July 2008 to 4 May 2009; For the 1.5 m deep thermokarst margin, temperatures were recorded from 10 April 2009 to 11 November 2009).

Figure 7 presents the simulated CH_4% in bubbles arriving at the top surface of Tube Dispenser Lake. As illustrated in section 3.2.1, bubbles produced at the thermokarst margin zones were more likely to contain higher percentages of CH_4 before being released to atmosphere (due to a higher density of high-flux ebullition seeps and more associated N_2 stripping). Meanwhile, the peak values of bubble CH_4 percentage occurred in summer for the nonthermokarst ebullition and in winter for the thermokarst ebullition. The simulated CH_4% is 92 ± 5% for the TD-TKM zone, 72 ± 20% for the TD-NTKM zone, and 56 ± 25% for the TD-CT zone. The comparison of bubble CH_4% between the SC-CT and TD-CT zones shows that the higher ebullition rates of the Tube Dispenser center leaded to higher CH_4 abundance in bubbles even though the centers of Lake Shuchi are much shallower, which supports our claim that ebullition rate (N_2 stripping) is the most important factor in determining CH_4 content fraction.

3.2.3. Goldstream Lake

Figure 8 compares the modeled and observed lake temperatures at a 1.5 m deep thermokarst margin and a 2.3 m deep lake center of Goldstream Lake, Alaska. For the lake center, temperature was measured and simulated at three layers: the water layer 1.5 m deep beneath water-air interface, the water-sediment interface, and the sediment layer 1 m deep beneath water-sediment interface. The mean error of simulated temperature is about 0.5°C for the water layer, 0.59°C for the water-sediment interface, and 0.21°C for the sediment layer. For the lake margin, temperature was measured and simulated at two layers: the water-sediment interface and the sediment layer 1 m deep beneath water-sediment interface. The mean error of simulations is about 1.05°C for the water-sediment interface and 0.27°C for the sediment layer. As implied, the horizontal heat exchange with peripheral permafrost at lake margins limited the warming of underlain talik, albeit the marginal zone has less water to impede heat penetration. Figure 8 discloses that the thermal maximum in different layers arrived in a chronological order with layer depth: from July in the midwater layer, August at the lake bottom to September in the superficial sediment layer, reflecting heat pulse transported downward from air to sediments in summer. *Burn* [2002] observed that the coldest water temperatures throughout the lakes in Richards Island, Canada occurred in late September, just before the formation

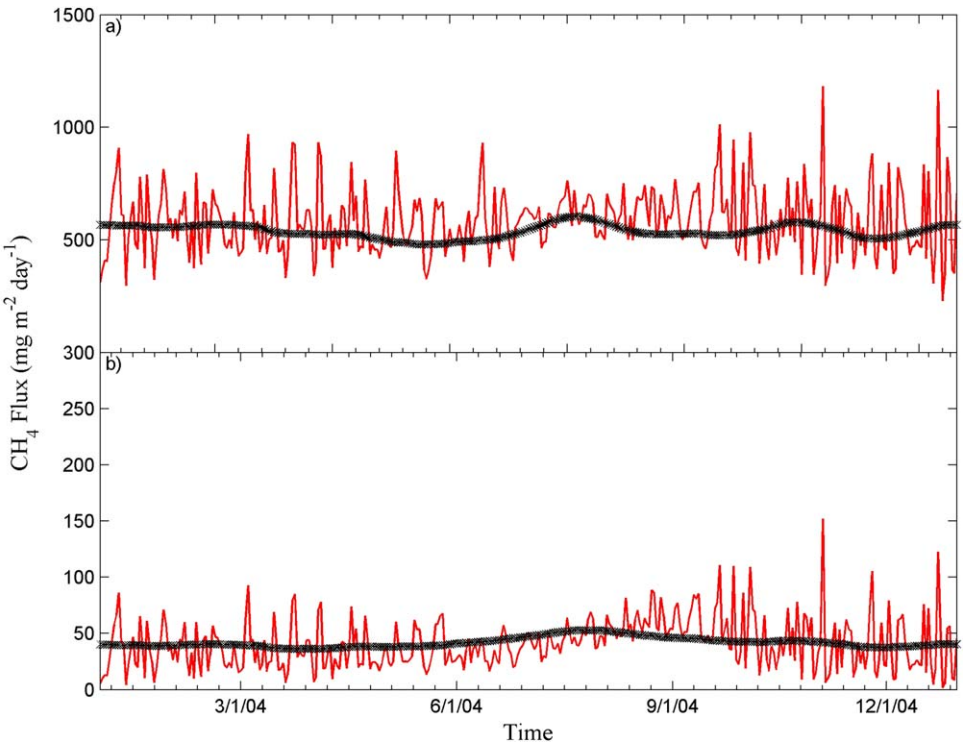

Figure 9. Comparison of the simulated and observed CH_4 fluxes at Goldstream Lake, Alaska on (a) CH_4 ebullition fluxes from the thermokarst margin zone GS-TKM; and (b) CH_4 ebullition fluxes from the lake center zone GS-CT. Ebullition fluxes only include ebullition from point-source seeps. Note different scales on the *Y* axis.

of ice cover, and with heat stored in surface sediments during summer diffusing back into the water column, the lake bottom warmed over winter. As shown in Figure 8, the similar thermal patterns can also be observed in this Alaskan lake: in late September the sinking of cold surface water cooled the lake bottom dramatically.

In Figure 9, we compare the simulated CH_4 ebullition fluxes to observations at a thermokarst margin zone with a mean depth of 1.5 m ("GS-TKM") and a nonthermokarst center zone with a mean depth of 2.3 m ("GS-CT") of Goldstream Lake from 1 January 2004 to 31 December 2004. With methanogenesis fueled by abundant Pleistocene-aged organic carbon from thawing retransported, yedoma-type permafrost [*Brosius et al*., 2012; *Greene et al*., 2014], CH_4 ebullition at the GS-TKM zone was much stronger than that in GS-CT. As the observed CH_4 fluxes have been smoothed, it is difficult to compare the simulated and observed diurnal variability of CH_4 ebullition. After processing simulations with a 2 week moving average filter, the mean daily error of modeled fluxes is 47.9 mg CH_4 m^{-2} d^{-1} for the GS-TKM zone and 6.3 mg CH_4 m^{-2} d^{-1} for the GS-CT zone. As in Tube Dispenser Lake, the maximum flux rate was modeled to occur in August, lagging 1 month behind the warmest day in 2003.

3.2.4. Lake Claudi and Toolik Lake

In Figure 10, we present the simulated CH_4 ebullition fluxes by comparison to observations at a thermokarst zone with a mean depth of 4.3 m ("CD-TK") and a nonthermokarst zone with a mean depth of 6.5 m ("CD-NTK") of Lake Claudi and a nonthermokarst center zone with a mean depth of 7.5 m ("TLK") of Toolik Lake, Alaska. Consistent with the TD-TKM zone, ebullition fluxes from CD-TK exhibit invariant base fluxes throughout the year and high flux maxima in the summer, owing to the origins of both temperature-insensitive CO_2 reduction and temperature-sensitive acetate fermentation. Because yedoma environments are more productive than nonyedoma environments in our Siberia and Alaska study lakes by supplying more ^{14}C-enriched carbon to lakes from both terrestrial and aquatic sources [*Walter Anthony et al*., 2014], the CH_4 emission magnitude in nonyedoma Toolik Lake was lower than in the yedoma lakes. Other reasons accounting for its lowest fluxes include potentially higher concentrations of other electron acceptors, i.e., iron and manganese [*Cornwell and Kipphut*, 1992]. By smoothing the simulated ebullition, we calculate the mean

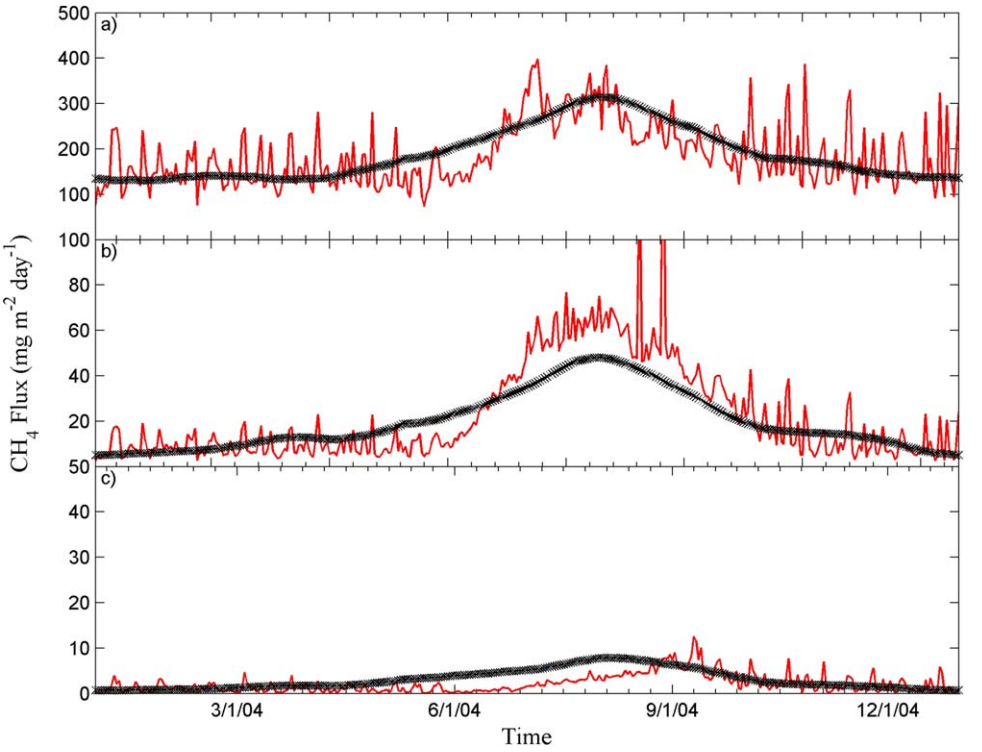

Figure 10. Comparison of the simulated and observed CH_4 fluxes at Claudi and Toolik Lake, Siberia on (a) CH_4 ebullition fluxes from the thermokarst zone of Lake Claudi (CD-TK); (b) CH_4 ebullition fluxes from the nonthermokarst zone of Lake Claudi (CD-NTK); and (c) CH_4 ebullition fluxes from the center zone of Toolik Lake (TLK). Ebullition fluxes only include ebullition from point-source seeps. Note different scales on the *Y* axis.

daily error of simulations is 22.8 mg CH_4 m^{-2} d^{-1} for the CD-TK zone, 6.7 mg CH_4 m^{-2} d^{-1} for the CD-NTK zone, and 1.3 mg CH_4 m^{-2} d^{-1} for the TLK zone. A linear regression involving the five flux simulations upon the three Alaskan lakes is presented in supporting information Figure S6. Relatively, the deviation between the modeled and observed CH_4 ebullition fluxes is low (high R^2), as smoothing has largely eliminated the diurnal variability of ebullition.

In Figure 11, the simulated CH_4% from three Alaskan lakes is compared. Due to strong ebullition, the two thermokarst zones (GS-TKM and CD-TK) have the highest CH_4 concentration in bubbles: 92 ± 6% and 80 ± 16%, respectively. The CH_4% of the three nonthermokarst zones is relatively low: 60 ± 22% for GS-CT, 53 ± 22% for CD-NTK, and 41 ± 26% for TLK. Since GS-CT and CD-NTK have comparable emission rates, the difference of their CH_4 content fraction should be attributed to the shallower water of the GS-CT zone (2.3 m deep versus 6.5 m deep). The lowest CH_4% in the nonthermokarst areas occurred in late fall, when ebullition fluxes dropped dramatically (reducing N_2 stripping) and ice layers were still thin.

3.3. Model Applicability to Other High-Latitude Lakes

This model was only validated by the observations collected from the thermokarst and nonthermokarst areas of several yedoma lakes and the center areas of a nonthermokarst nonyedoma lake. However, it is feasible to adapt the model to estimate CH_4 emissions from other types of unpolluted high-latitude freshwater lakes, such as peatland lakes. For peatland thaw lakes, such as those that occur in the Hudson Bay Lowlands [*Sannel and Kuhry*, 2011], a two-carbon-pool model should be still well-suited. In the deep sediments, old organic matter mobilized from previous permafrost can provide additional labile substrate to methanogens. In the surface sediments, methanogenesis can rely on newly deposited organic materials, the labile carbon content of which decreases with depth. Thus, CH_4 emissions from peatland thaw lakes could also be quantified by our model with proper lake-specific parameters employed, i.e., the regional mean densities of total carbon in the permafrost and in the lake surface sediments. When a peatland lake

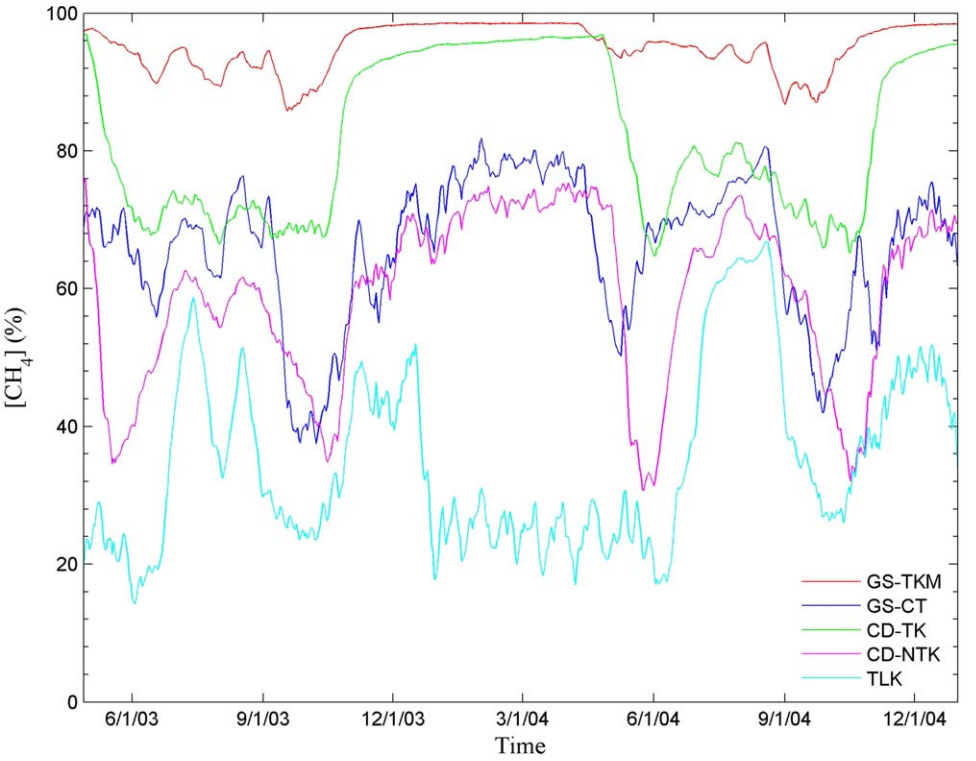

Figure 11. The variability of modeled CH_4 percentage concentrations in bubbles released from Goldstream Lake, Claudi Lake, and Toolik Lake, Alaska during 28 April 2003 and 31 December 2004 (for yedoma lakes, the measured CH_4% was from 73% to 90% at thermokarst margins and 63.8 $\pm$ 16.1% at other areas; for nonyedoma lakes, the measured CH_4% was 63.8 $\pm$ 16.1%).

is not a thaw lake, CH_4 production could mainly flourish in the surface sediments but be fueled by large amounts of organic matter added by active bank erosion or within-lake primary production. The enhancement of carbon transport by bank erosion can be represented by the multiplier α_{erode} of the ^{14}C-enriched carbon pool. In this circumstance, α_{erode} should be either derived from the total carbon stock of the lake's highly eroded margins or calibrated with the observed CH_4 ebullition fluxes. The deposition of organic matter from within-lake productivity can be modeled by parameterizing the production and respiration of within-lake organisms in both littoral and profundal zones [*Hanson et al*., 2004; *Stefan and Fang*, 1994; *Zhuang et al*., 2004].

Additionally, following modeling methods of *Zhuang et al*. [2004] and *Tang et al*. [2010], it might be reasonable to take the transport of CH_4 through the aerenchyma of plants into account when the studied lakes contain vascular plants.

4. Conclusions

We develop a process-based lake biogeochemical model involving physical and biogeochemical processes to quantify CH_4 ebullition and diffusive fluxes from pan-arctic lakes. The model well simulates temperature profiles in the lake water and sediment columns, CH_4 concentration profiles in the water column, and CH_4 ebullition emissions at Shuchi Lake and Tube Dispenser Lake of Siberia and Goldstream Lake, Claudi Lake, and Toolik Lake of Alaska. The mean errors of temperature simulations and dissolved CH_4 simulations in most cases are less than 1°C and 0.2 μM, respectively. The correlations between the modeled and observed CH_4 fluxes are close to 1.0 for both Siberian and Alaskan lakes. The model supports the argument that CH_4 percentage concentration in bubbles is controlled by ebullition magnitude and demonstrates that lake depth and ice cover formation are also important factors. As observed in the studied lakes, the simulated bubble fluxes from the thermokarst areas are much higher than from the nonthermokarst areas. And the short-term variations of kotara and hotspot ebullition could be controlled by biogeochemical factors more complex than this model, such as microbial metabolism. Overall, since the magnitude of ebullition is well

constrained in the simulations, the model appears to be capable to estimate CH_4 emissions from pan-arctic lakes at the regional scale.

Acknowledgments
The authors appreciate the insightful comments from Daniel McGinnis and two anonymous reviewers. The authors also thank D. Draluk, D. Vas, and A. Strohm for assistance with field measurements. The research was funded by a DOE SciDAC project and an Abrupt Climate Change project (DE-FG02–08ER64599 to Q.Z.). This study was also supported through projects funded by the NASA Land Use and Land Cover Change program (NASA-NNX09AI26G to Q.Z.), NASA Carbon Cycle Science (NASA-NNX11AH20G to Q.Z.), the NSF Division of Information and Intelligent Systems (NSF-1028291 to Q.Z.), the NSF Carbon and Water in the Earth Program (NSF-0630319 to Q.Z.), and the NSF ARC-1304823 and OPP-1107892. This research was also in part supported by the Director, Office of Science, Office of Biological and Environmental Research of the US Department of Energy under contract DE-AC02–05CH11231 as part of their Earth System Modeling Program. The data for this paper are available at European Center for Medium-Range Weather Forecasts (ECMWF) Interim reanalysis (ERA-Interim) (http://apps.ecmwf.int/datasets/), at Bolin Centre Database for the Northern Circumpolar Soil Carbon Database (http://bolin.su.se/data/ncscd/), NCEAS project 10646 (https://www.nceas.ucsb.edu/projects/10645), and Arctic Long Term Ecological Research Site (ARC LTER) data server (http://ecosystems.mbl.edu/ARC/datacatalog.html).

References

Algar, C. K., and B. P. Boudreau (2009), Transient growth of an isolated bubble in muddy, fine-grained sediments, *Geochim. Cosmochim. Acta*, *73*(9), 2581–2591.

Audry, S., O. S. Pokrovsky, L. S. Shirokova, S. N. Kirpotin, and B. Dupr (2011), Organic matter mineralization and trace element post-depositional redistribution in Western Siberia thermokarst lake sediments, *Biogeosciences*, *8*, 3341–3358.

Baird, A. J., C. W. Beckwith, S. Waldron, and J. M. Waddington (2004), Ebullition of methane-containing gas bubbles from near-surface Sphagnum peat, *Geophys. Res. Lett.*, *31*, L21505, doi:10.1029/2004GL021157.

Barber, R. (2007), Methanogenesis: Ecology, in *Encyclopedia of Life Sciences*, edited by Roland Jansson, pp. 1–8, John Wiley, N. Y., doi: 10.1002/9780470015902.a0000475.pub2.

Bastviken, D., J. Cole, M. Pace, and L. Tranvik (2004), Methane emissions from lakes: Dependence of lake characteristics, two regional assessments, and a global estimate, *Global Biogeochem. Cycles*, *18*, GB4009, doi:10.1029/2004GB002238.

Bastviken, D., L. Tranvik, J. Downing, P. M. Crill, and A. Enrich-Prast (2011), Freshwater methane emissions offset the continental carbon sink, *Science*, *331*(6013), 50–50.

Benoy, G., K. Cash, E. McCauley, and F. Wrona (2007), Carbon dynamics in lakes of the boreal forest under a changing climate, *Environ. Rev.*, *15*, 175–189, doi:10.1139/A07-006.

Brosius, L. S., K. M. Walter Anthony, G. Grosse, J. P. Chanton, L. M. Farquharson, P. P. Overduin, and H. Meyer (2012), Using the deuterium isotope composition of permafrost meltwater to constrain thermokarst lake contributions to atmospheric CH_4 during the last deglaciation, *J. Geophys. Res.*, *117*, G01022, doi:10.1029/2011JG001810.

Burden, R. L., J. D. Faires, and A. C. Reynolds (1978), *Numerical Analysis*, pp. 254, Prindle, Weber and Schmidt Inc., Boston, Mass.

Burn, C. (2002), Tundra lakes and permafrost, Richards Island, western Arctic coast, Canada, *Can. J. Earth Sci.*, *39*, 1281–1298, doi:10.1139/E02–035.

Canham, C., M. Pace, M. J. Papaik, A. V. B. Primack, K. M. Roy, R. J. Maranger, R. P. Curran, and D. M. Spada (2004), A spatially explicit watershed-scale analysis of dissolved organic carbon in Adirondack lakes, *Ecol. Appl.*, *14*(3), 839–854.

Casper, P., S. Maberly, G. Hall, and B. Finlay (2000), Fluxes of methane and carbon dioxide from a small productive lake to the atmosphere, *Biogeochemistry*, *49*(1), 1–19.

Chanton, J. P., C. S. Martens, and C. A. Kelley (1989), Gas transport from methane-saturated tidal freshwater and wetland sediments, *Limnol. Oceanogr.*, *34*, 807–819.

Cicerone, R., and R. Oremland (1988), Biogeochemical aspects of atmospheric methane, *Global Biogeochem. Cycles*, *2*(4), 299–327.

Cole, J. J., Y. T. Prairie, N. F. Caraco, W. H. McDowell, L. J. Tranvik, R. G. Striegl, and J. Melack (2007). Plumbing the global carbon cycle: Integrating inland waters into the terrestrial carbon budget, *Ecosystems*, *10*(1), 172–185, doi:10.1007/s10021-006-9013-8.

Cornwell, J. C., and G. W. Kipphut (1992), Biogeochemistry of manganese- and iron-rich sediments in Toolik Lake, Alaska, *Hydrobiologia*, *240*(1–3), 45–59, doi:10.1007/BF00013451.

Coulthard, T., A. Baird, J. Ramirez, and J. M. Waddington (2009), Methane dynamics in peat: Importance of shallow peats and a novel reduced-complexity approach for modeling ebullition, in *Carbon Cycle in Northern Peatlands*, vol. 2, edited by A. J. Baird, pp. 173–185, AGU, Washington, D. C.

Davison, A. C., and D. V. Hinkley (1997), *Bootstrap Methods and Their Application*, Cambridge Univ. Press, Cambridge, N. Y.

Dee, D. P., and S. Uppala (2009), Variational bias correction of satellite radiance data in the ERA-Interim reanalysis, *Q. J. R. Meteorol. Soc.*, *135*, 1830–1841.

Denman, K. L., et al. (2007), Couplings between changes in the climate system and biogeochemistry, in *Climate Change 2007: The physical cscience basis, in Contribution of Working Group I to the Fourth Assessment Report of the Intergovernmental Panel on Climate Change*, edited by S. Solomon et al., chap. 7, pp. 501–587, Cambridge Univ. Press, Cambridge, U. K.

De Vries, D. A. (1963), Thermal properties of soils, in *Physics of Plant Environment*, edited by W. R. van Wijk, pp. 210–235, North-Holland, Amsterdam.

Dlugokencky, E. J., B. P. Walter, K. A. Masarie, P. M. Lang, and E. S. Kasischke (2001), Measurements of an anomalous global methane increase during 1998, *Geophys. Res. Lett.*, *28*(3), 499–502.

Dlugokencky, E. J., et al. (2009), Observational constraints on recent increases in the atmospheric CH4 burden, *Geophys. Res. Lett.*, *36*, L18803, doi:10.1029/2009GL039780.

Donahue, R. L., R. W. Miller, and J. C. Shickluna (1983), *Soils: An introduction to Soils and Plant Growth*, 5th ed., pp. 58, Prentice Hall, Englewood Cliffs, N. J.

Duan, Q., S. Sorooshian, and V. Gupta (1994), Optimal use of the SCE-UA global optimization method for calibrating watershed models, *J. Hydrol.*, *158*, 265–284.

Etheridge, D. M., L. P. Steele, R. J. Francey, and R. L. Langenfelds (1998), Atmospheric methane between 1000 A.D. and present: Evidence of anthropogenic emissions and climatic variability, *J. Geophys. Res.*, *103*(D13), 15,979–15,993.

Fang, X., and H. G. Stefan (1994), Temperature and dissolved oxygen simulations in a lake with ice cover, *Proj. Rep.*, *365*(65). U.S. Environmental Protection Agency, Environmental Research Laboratory, Duluth, Minn.

Fang, X., and H. G. Stefan (1998), Temperature variability in lake sediments, *Water Resour. Res.*, *34*(4), 717–729.

Farouki, O. T. (1981), The thermal properties of soils in cold regions, Cold Regions Science and Technology, *5*(1), 61–75.

Ferland, M.-E., P. A. del Giorgio, C. R. Teodoru, and Y. T. Prairie (2012), Long-term C accumulation and total C stocks in boreal lakes in northern Québec, *Global Biogeochem. Cycles*, *26*, GB0E04, doi:10.1029/2011GB004241.

Ferland, M.-E., Y. T. Prairie, C. Teodoru, and P. A. del Giorgio (2014), Linking organic carbon sedimentation, burial efficiency and long-term accumulation in boreal lakes, *J. Geophys. Res. Biogeosci.*, *119*, 836–847, doi:10.1002/2013JG002345.

Fisher, R. E., et al. (2011), Arctic methane sources: Isotopic evidence for atmospheric inputs, *Geophys. Res. Lett.*, *38*, L21803, doi:10.1029/2011GL049319.

Forster, P., et al. (2007), Changes in atmospheric constituents and in radiative forcing, in *Climate Change 2007: The Physical Science Basis. Contribution of Working Group I to the Fourth Assessment Report of the Intergovernmental Panel on Climate Change*, edited by S. Solomon et al., chap. 2, pp. 131–234, Cambridge Univ. Press, Cambridge, U. K.

Gao, X., C. Adam Schlosser, A. Sokolov, K. M. Walter Anthony, Q. Zhuang, and D. Kicklighter (2013), Permafrost degradation and methane: Low risk of biogeochemical climate-warming feedback, *Environ. Res. Lett.*, *8*(3), 035014, doi:10.1088/1748-9326/8/3/035014.

Giblin, A., C. Luecke, and G. Kling (2010), Physical and chemical data for various lakes near Toolik Research Station, Arctic LTER Summer 2007. Long Term Ecological Research Network, N. M. [Available at http://tropical.lternet.edu/knb/metacat/knb-lter-arc.10073.4/lter.]
Greene, S., K. M. Walter Anthony, D. Archer, A. Sepulveda-Jauregui, and K. Martinez-Cruz (2014), Modeling the impediment of methane ebullition bubbles by seasonal lake ice, *Biogeosciences*, *11*, 6791–6811, doi:10.5194/bg-11-6791-2014.
Hansen, J., et al. (2007), Dangerous human-made interface with climate: A GISS modelE study, *Atmos. Chem. Phys.*, *7*(9), 2287–2312.
Hanson, P. C., A. I. Pollard, D. L. Bade, K. Predick, S. R. Carpenter, and J. A. Foley (2004), A model of carbon evasion and sedimentation in temperate lakes, *Global Change Biol.*, *10*, 1285–1298.
Hansson, K., J. Šimůnek, M. Mizoguchi, L. Lundin, and M. T. van Genuchten (2004), Water flow and heat transport in frozen soil: Numerical solution and freeze-thaw applications, *Vadose Zone J.*, *3*(2), 693–704.
Harden, J. W., et al. (2012), Field information links permafrost carbon to physical vulnerabilities of thawing, *Geophys. Res. Lett.*, *39*, L15704, doi:10.1029/2012GL051958.
Hillel, D. (1980), *Fundamentals of Soil Physics*, pp. 10–11, 161–162, Academic, London, U. K.
Hodgkins, S. B., M. M. Tfaily, C. K. McCalley, T. A. Logan, P. M. Crill, S. R. Saleska, V. I. Rich, and J. P. Chanton (2014), Changes in peat chemistry associated with permafrost thaw increase greenhouse gas production, *Proc. Natl. Acad. Sci. U. S. A.*, *111*, 5819–5824, doi:10.1073/pnas.1314641111.
Hostetler, S. W., and P. J. Bartlein (1990), Simulation of lake evaporation with application to modeling lake level variations of Harney-Malheur Lake, Oregon, *Water Resour. Res.*, *26*(10), 2603–2612.
Hugelius, G., et al. (2013), A new data set for estimating organic carbon storage to 3 m depth in soils of the northern circumpolar permafrost region, *Earth Syst. Sci. Data*, *5*, 393–402.
Intergovernmental Panel on Climate Change (2013), Climate change 2013, in *The Physical Science Basis, Contribution of Working Group I to the Fifth Assessment Report of the Intergovernmental Panel on Climate change*, edited by T. F. Stocker et al., Cambridge Univ. Press, Cambridge, U. K.
Isaksen, I. S. A., M. Gauss, G. Myhre, K. M. Walter Anthony, and C. Ruppel (2011), Strong atmospheric chemistry feedback to climate warming from Arctic methane emissions, *Global Biogeochem. Cycles*, *25*, GB2002, doi:10.1029/2010GB003845.
Johnston, C. N. (1939), Heat conductivity of soil governs heat losses from heated oil lines, *Petrol. Eng.*, *9*(1), 41.
Kelly, C. A., et al. (1997), Increases in fluxes of greenhouse gases and methyl mercury following flooding of an experimental reservoir, *Environ. Sci. Technol.*, *31*(5), 1334–1344, doi:10.1021/es9604931.
Kessler, M. A., L. Plug, and K. M. Walter Anthony (2012), Simulating the decadal to millennial scale dynamics of morphology and sequestered carbon mobilization of two thermokarst lakes in N.W. Alaska, *J. Geophys. Res.*, *117*, G00M06, doi:10.1029/2011JG001796.
Kling, G., G. W. Kipphut, and M. C. Miller (1992), The flux of CO_2 and CH_4 from lakes and rivers in arctic Alaska, *Hydrobiologia*, *240*, 23–36.
Kort, E. A., et al. (2012), Atmospheric observations of Arctic Ocean methane emissions up to 82° north, *Nat. Geosci.*, *5*(5), 318–321, doi:10.1038/ngeo1452.
Leifer, I., and R. K. Patro (2002), The bubble mechanism for methane transport from the shallow sea bed to the surface: A review and sensitivity study, *Cont. Shelf Res.*, *22*(16), 2409–2428.
Liang, J.-H., J. C. McWilliams, P. P. Sullivan, and B. Baschek (2011), Modeling bubbles and dissolved gases in the ocean, *J. Geophys. Res.*, *116*, C03015, doi:10.1029/2010JC006579.
Ling, F., and T. Zhang (2003), Numerical simulation of permafrost thermal regime and talik development under shallow thaw lakes on the Alaskan Arctic Coastal Plain, *J. Geophys. Res.*, *108*(D16), 4511, doi:10.1029/2002JD003014.
MacDougall, A. H., C. A. Avis, and A. J. Weaver (2012), Significant contribution to climate warming from the permafrost carbon feedback, *Nat. Geosci.*, *5*(10), 719–721, doi:10.1038/ngeo1573.
MacIntyre, S., J. P. Fram, P. J. Kushner, N. D. Bettez, W. J. O. Brien, J. E. Hobbie, and G. W. Kling (2009), Climate-related variations in mixing dynamics in an Alaskan arctic lake, *Limnol. Oceanogr. Methods*, *54*, 2401–2417.
MacKay, M. D., et al. (2009), Modeling lakes and reservoirs in the climate system, *Limnol. Oceanogr. Methods*, *54*(6), 2315–2329.
McGinnis, D. F., J. Greinert, Y. Artemov, S. E. Beaubien, and A. Wüest (2006), Fate of rising methane bubbles in stratified waters: How much methane reaches the atmosphere? *J. Geophys. Res.*, *111*, C09007, doi:10.1029/2005JC003183.
Nakagawa, F., N. Yoshida, Y. Nojiri, and V. Makarov (2002), Production of methane from alasses in eastern Siberia: Implications from its ^{14}C and stable isotopic compositions, *Global Biogeochem. Cycles*, *16*(3), 1041, doi:10.1029/2000GB001384.
Riera, J. L., J. E. Schindler, and T. K. Kratz (1999), Seasonal dynamics of carbon dioxide and methane in two clear-water lakes and two bog lakes in northern Wisconsin, U.S.A., *Can. J. Fish. Aquat. Sci.*, *56*, 265–274.
Riordan, B., D. Verbyla, and A. D. McGuire (2006), Shrinking ponds in subartic Alaska based on 1950–2002 remotely sensed images, *J. Geophys. Res.*, *111*, G04002, doi:10.1029/2005JG000150.
Rudd, J. W. M., R. D. Hamilton, and N. E. R. Campbell (1978), Methane cycling in a eutrophic Canadian Shield lake and its effects on whole lake metabolism, *Limnol. Oceanogr.*, *23*, 337–348.
Saltelli, A. (2002), Making best use of model evaluations to compute sensitivity indices, *Comput. Phys. Commun.*, *145*(2), 280–297, doi:10.1016/S0010–4655(02)00280-1.
Sannel, A. B. K., and P. Kuhry (2011), Warming-induced destabilization of peat plateau/thermokarst lake complexes, *J. Geophys. Res.*, *116*, G03035, doi:10.1029/2010JG001635.
Scandella, B. P., C. Varadharajan, H. F. Hemond, C. Ruppel, and R. Juanes (2011a), A conduit dilation model of methane venting from lake sediments, *Geophys. Res. Lett.*, *38*, L06408, doi:10.1029/2011GL046768.
Scandella, B. P., H. Hemond, C. Ruppel, and R. Juanes (2011b), Escape paths for biogenic methane gas in lake sediments: Morphology and dynamics, Abstract H21B-1089 presented at Fall Meeting, AGU, San Francisco, Calif., 5–9 Dec.
Schädel, C., E. A. G. Schuur, R. Bracho, B. Elberling, C. Knoblauch, H. Lee, Y. Luo, G. R. Shaver, and M. R. Turetsky (2014), Circumpolar assessment of permafrost C quality and its vulnerability over time using long-term incubation data, *Global Change Biol.*, *20*(2), 641–652.
Schirrmeister, L., G. Grosse, S. Wetterich, P. P. Overduin, J. Strauss, E. A. G. Schuur, and H. Hubberten (2011), Fossil organic matter characteristics in permafrost deposits of the northeast Siberian Arctic, *J. Geophys. Res.*, *116*, G00M02, doi:10.1029/2011JG001647.
Schulz, S., H. Matsuyama, and R. Conrad (1997), Temperature dependence of methane production from different precursors in a profundal sediment (Lake Constance), *FEMS Microbiol. Ecol.*, *22*, 207–213, doi:10.1111/j.1574-6941.1997.tb00372.x.
Schuur, E. A. G., B. Abbott, and the Permafrost Carbon Network (2011), High risk of permafrost thaw, *Nature*, *480*, 32–33.
Segers, R. (1998), Methane production and methane consumption: A review of processes underlying wetland methane fluxes, *Biogeochemistry*, *41*(1), 23–51.
Semiletov, I. P. (1999), Aquatic sources and sinks of CO_2 and CH_4 in the polar regions, *J. Atmos. Sci.*, *56*, 286–306.

Sepulveda-Jauregui, A., K. M. Walter Anthony, K. Martinez-Cruz, S. Greene, and F. Thalasso (2014), Methane and carbon dioxide emissions from 40 lakes along a north-south latitudinal transect in Alaska, *Biogeosci. Discuss.*, *11*, 13,251–13,307.

Shampine, L. F., S. Thompson, J. A. Kierzenka, and G. D. Byrne (2005), Non-negative solutions of ODEs, *Appl. Math. Comput.*, *170*(1), 556–569, doi:10.1016/j.amc.2004.12.011.

Sobol', I. M. (1993), Sensitivity analysis for non-linear mathematical models, *Math. Modell. Comput. Exp.*, *1*, 407–414.

Sobol', I. M. (2001), Global sensitivity indices for nonlinear mathematical models and their Monte Carlo estimates, *Math. Comput. Simul.*, *55*(1–3), 271–280.

Stefan, H. G., and X. Fang (1994), Dissolved oxygen model for regional lake analysis, *Ecol. Modell.*, *71*(1–3), 37–68, doi:10.1016/0304-3800(94)90075-2.

Stepanenko, V. M., E. E. Machul'skaya, M. V. Glagolev, and V. N. Lykossov (2011), Numerical modeling of methane emissions from lakes in the permafrost zone, Izvestiya, *Atmos. Oceanic Phys.*, *47*(2), 252–264.

Strack, M., E. Kellner, and J. M. Waddington (2005), Dynamics of biogenic gas bubbles in peat and their effects on peatland biogeochemistry, *Global Biogeochem. Cycles*, *19*, GB1003, doi:10.1029/2004GB002330.

Subin, Z. M., W. J. Riley, and D. Mironov (2012), An improved lake model for climate simulations: Model structure, evaluation, and sensitivity analyses in CESM1, *J. Adv. Model. Earth Syst.*, *4*, M02001, doi:10.1029/2011MS000072.

Tang, J., and Q. Zhuang (2009), A global sensitivity analysis and Bayesian inference framework for improving the parameter estimation and prediction of a process-based Terrestrial Ecosystem Model, *J. Geophys. Res.*, *114*, D15303, doi:10.1029/2009JD011724.

Tang, J., Q. Zhuang, R. D. Shannon, and J. R. White (2010), Quantifying wetland methane emissions with process-based models of different complexities, *Biogeosciences*, *7*(11), 3817–3837, doi:10.5194/bg-7-3817-2010.

Tarnocai, C., J. G. Canadell, E. A. G. Schuur, P. Kuhry, G. Mazhitova, and S. Zimov (2009), Soil organic carbon pools in the northern circumpolar permafrost region, *Global Biogeochem. Cycles*, *23*, GB2023, doi:10.1029/2008GB003327.

Thorpe, S. A. (1982), On the clouds of bubbles formed by breaking wind-waves in deep water, and their role in air-sea gas transfer, *Philos. Trans. R. Soc. London A*, *304*, 155–210.

Torrey, M. S., and G. F. Lee (1976), Nitrogen fixation in Lake Mendota, Madison, Wisconsin, *Limnol. Oceanogr.*, *21*(3), 365–378.

van Bodegom, P., F. Stams, L. Mollema, B. Sara, and P. Leffelaar (2001), Methane oxidation and the competition for oxygen in the rice rhizosphere, *Appl. Environ. Microbiol.*, *67*(8), 3586–3597, doi:10.1128/AEM.67.8.3586-3597.2001.

van Huissteden, J., C. Berrittella, F. J. W. Parmentier, Y. Mi, T. C. Maximov, and A. J. Dolman (2011), Methane emissions from permafrost thaw lakes limited by lake drainage, *Nat. Clim. Change*, *1*(2), 119–123, doi:10.1038/nclimate1101.

Varadharajan, C., and H. F. Hemond (2012), Time-series analysis of high-resolution ebullition fluxes from a stratified, freshwater lake, *J. Geophys. Res.*, *117*, G02004, doi:10.1029/2011JG001866.

Walter, P., and M. Heimann (2000), A process-based, climate-sensitive model to derive CH_4 emissions from natural wetlands: Application to five wetland sites, sensitive to model parameters, and climate, *Global Biogeochem. Cycles*, *14*(3), 745–765.

Walter, K. M., S. A. Zimov, J. P. Chanton, D. Verbyla, and F. S. Chapin III (2006), Methane bubbling from Siberian thaw lakes as a positive feedback to climate warming, *Nature*, *443*(7107), 71–5, doi:10.1038/nature05040.

Walter, K. M., L. C. Smith, and F. S. Chapin III (2007), Methane bubbling from northern lakes: Present and future contributions to the global methane budget, *Philos. Trans. R. Soc. A*, *365*(1856), 1657–76, doi:10.1098/rsta.2007.2036.

Walter, K. M., J. P. Chanton, F. S. Chapin III, E. A. G. Schuur, and S. A. Zimov (2008), Methane production and bubble emissions from arctic lakes: Isotopic implications for source pathways and ages, *J. Geophys. Res.*, *113*, G00A08, doi:10.1029/2007JG000569.

Walter Anthony, K. M., and P. Anthony (2013), Constraining spatial variability of methane ebullition seeps in thermokarst lakes using point process models, *J. Geophys. Res. Biogeosci.*, *118*, 1015–1034, doi:10.1002/jgrg.20087.

Walter Anthony, K. M., D. A. Vas, L. Brosius, F. S. Chapin III, S. A. Zimov, and Q. Zhuang (2010), Estimating methane emissions from northern lakes using ice-bubble surveys, *Limnol. Oceanogr. Methods*, 592–609.

Walter Anthony, K. M., P. Anthony, G. Grosse, and J. Chanton (2012), Geologic methane seeps along boundaries of Arctic permafrost thaw and melting glaciers, *Nat. Geosci.*, *5*(6), 419–426, doi:10.1038/ngeo1480.

Walter Anthony, K. M., et al. (2014), A shift of thermokarst lakes from carbon sources to sinks during the Holocene epoch, *Nature*, *511*, 452–456, doi:10.1038/nature13560.

West, J. J., and L. J. Plug (2008), Time-dependent morphology of thaw lakes and taliks in deep and shallow ground ice, *J. Geophys. Res.*, *113*, F01009, doi:10.1029/2006JF000696.

Whalen, S. C., W. S. Reeburgh, and K. A. Sandbeck (1990), Rapid methane oxidation in a landfill cover soil, *Appl. Environ. Microbiol.*, *56*(11), 3405–3411.

Wik, M., B. F. Thornton, D. Bastviken, S. MacIntyre, R. K. Varner, and P. M. Crill (2014), Energy input is primary controller of methane bubbling in subarctic lakes, *Geophys. Res. Lett.*, *41*, 555–560, doi:10.1002/2013GL058510.

Woolf, D. K., and S. Thorpe (1991), Bubbles and the air-sea exchange of gases in near-saturation conditions, *J. Mar. Res.*, *49*(3), 435–466.

Wüest, A., G. Piepke, and D. C. Van Senden (2000), Turbulent kinetic energy balance as a tool for estimating vertical diffusivity in wind-forced stratified waters, *Limnol. Oceanogr.*, *45*(6), 1388–1400.

Zhuang, Q., J. M. Melillo, D. W. Kicklighter, R. G. Prinn, A. D. McGuire, P. A. Steudler, B. S. Felzer, and S. Hu (2004), Methane fluxes between terrestrial ecosystems and the atmosphere at northern high latitudes during the past century: A retrospective analysis with a process-based biogeochemistry model, *Global Biogeochem. Cycles*, *18*, GB3010, doi:10.1029/2004GB002239.

Zimov, S. A., Y. V. Voropaev, I. P. Semiletov, S. P. Davidov, S. F. Prosiannikov, F. S. Chapin III, M. C. Chapin, S. Trumbore, and S. Tyler (1997), North Siberian lakes: A methane source fueled by Pleistocene carbon, *Science*, *277*(5327), 800–802, doi:10.1126/science.277.5327.800.

Zimov, S. A., Y. V. Voropaev, S. P. Davydov, G. M. Zimova, A. I. Davydova, F. S. Chapin III, and M. C. Chapin (2001), Flux of methane from North Siberian aquatic systems: Influence on atmospheric methane, in *Permafrost Response on Economic Development, Environmental Security and Natural Resources*, edited by R. Paepe and V. Melnikov, pp. 515–524, Kluwer Acad., Hague, Netherlands.